1 **Evaluating Nitrogen Cycling in Terrestrial Biosphere Models: Implications for the Future**
2 **Terrestrial Carbon Sink**

3 Sian Kou-Giesbrecht[1], Vivek Arora[1], Christian Seiler[2], Almut Arneth[3], Stefanie Falk[4], Atul Jain[5],
4 Fortunat Joos[6], Daniel Kennedy[7], Jürgen Knauer[8], Stephen Sitch[9], Michael O'Sullivan[9], Naiqing
5 Pan[10], Qing Sun[6], Hanqin Tian[10], Nicolas Vuichard[11], and Sönke Zaehle[12]

6 [1]Canadian Centre for Climate Modelling and Analysis, Climate Research Division, Environment
7 Canada, Victoria, Canada

8 [2]School of Environmental Studies, Queen's University, Kingston, Canada

9 [3]Karlsruhe Institute of Technology, Atmospheric Environmental Research, Garmisch-
10 Partenkirchen, Germany

11 [4]Department für Geographie, Ludwig-Maximilians-Universität Munich, München, Germany

12 [5]Department of Atmospheric Sciences, University of Illinois Urbana-Champaign, Urbana, USA

13 [6]Climate and Environmental Physics, Physics Institute and Oeschger Centre for Climate Change
14 Research, University of Bern, Bern, Switzerland

15 [7]National Center for Atmospheric Research, Climate and Global Dynamics, Terrestrial Sciences
16 Section, Boulder, USA

17 [8]Hawkesbury Institute for the Environment, Western Sydney University, Penrith, Australia

18 [9]Faculty of Environment, Science and Economy, University of Exeter, Exeter, UK

19 [10]Schiller Institute for Integrated Science and Society, Department of Earth and Environmental
20 Sciences, Boston College, Chestnut Hill, USA

21 [11]Laboratoire des Sciences du Climat et de l'Environnement, LSCE-IPSL (CEA-CNRS-UVSQ),
22 Université Paris-Saclay, Gif-sur-Yvette, France

23 [12]Max Planck Institute for Biogeochemistry, Jena, Germany

24 *Correspondence to:* Sian Kou-Giesbrecht (sian.kougiesbrecht@ec.gc.ca)

25

26 **Abstract**

27 Terrestrial carbon (C) sequestration is limited by nitrogen (N), a constraint that could
28 intensify under CO_2 fertilisation and future global change. The terrestrial C sink is estimated to
29 currently sequester approximately a third of annual anthropogenic CO_2 emissions based on an
30 ensemble of terrestrial biosphere models, which have been evaluated in their ability to reproduce
31 observations of the C, water, and energy cycles. However, their ability to reproduce observations
32 of N cycling and thus the regulation of terrestrial C sequestration by N has been largely
33 unexplored. Here, we evaluate an ensemble of terrestrial biosphere models with coupled C-N
34 cycling and their performance at simulating N cycling, outlining a framework for evaluating N
35 cycling that can be applied across terrestrial biosphere models. We find that models exhibit

36 significant variability across N pools and fluxes, simulating different magnitudes and trends over
37 the historical period, despite their ability to generally reproduce the historical terrestrial C sink.
38 This suggests that the underlying N processes that regulate terrestrial C sequestration operate
39 differently across models and may not be fully captured. Furthermore, models tended to
40 overestimate tropical biological N fixation, vegetation C:N ratio, and soil C:N ratio but
41 underestimate temperate biological N fixation relative to observations. However, there is
42 significant uncertainty associated with measurements of N cycling processes given their scarcity
43 (especially relative to those of C cycling processes) and their high spatiotemporal variability.
44 Overall, our results suggest that terrestrial biosphere models that represent coupled C-N cycling
45 (let alone those without a representation of N cycling) could be overestimating C storage per unit
46 N, which could lead to biases in projections of the future terrestrial C sink under CO_2 fertilisation
47 and future global change. More extensive observations of N cycling processes are crucial to
48 evaluate N cycling and its impact on C cycling as well as guide its development in terrestrial
49 biosphere models.

50

Plain Language Summary

52   Nitrogen (N) is an essential limiting nutrient to terrestrial carbon (C) sequestration. We
53 evaluate N cycling in an ensemble of terrestrial biosphere models. We find that they simulate
54 significant variability in N processes. Models tended to overestimate C storage per unit N in
55 vegetation and soil, which could have consequences for projecting the future terrestrial C sink.
56 However, N cycling measurements are highly uncertain and more are necessary to guide the
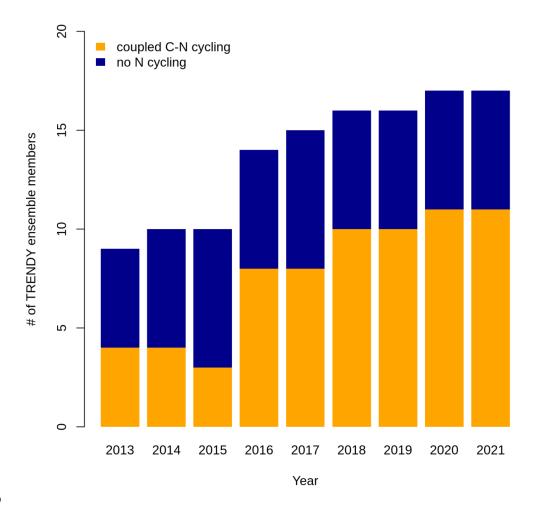57 development of N cycling in models.

58

1 Introduction

60   The terrestrial biosphere is estimated to currently sequester approximately a third of
61 anthropogenic CO_2 emissions by the Global Carbon Project (GCP) (Friedlingstein et al., 2022).
62 The GCP annually reports an estimate of the global carbon (C) budget which includes an
63 estimate of the atmosphere-land CO_2 flux, i.e., the terrestrial C sink, based on simulations of an
64 ensemble of terrestrial biosphere models – the trends in the land carbon cycle project (TRENDY)
65 ensemble. In recent years, the majority of the models within the TRENDY ensemble have
66 incorporated a representation of coupled C and nitrogen (N) cycling given the empirically
67 established importance of N limitation of vegetation growth (Elser et al., 2007; Fernández-
68 Martínez et al., 2014; LeBauer and Treseder, 2008; Wright et al., 2018): whereas only four out of
69 nine models represented coupled C-N cycling in the 2013 GCP, 11 out of 16 models represented
70 coupled C-N cycling in the 2022 GCP (Figure 1). Capturing N constraints on C cycling is critical
71 for realistically simulating the terrestrial C sink, which arises from the combined effects of
72 concurrently acting global change drivers that are each modulated by N: CO_2 fertilisation is
73 limited by N (Terrer et al., 2019; Wang et al., 2020a), intensifying N deposition increases N
74 supply (O'Sullivan et al., 2019; Wang et al., 2017), rising temperature and varying precipitation
75 modulate decomposition and soil N availability (Liu et al., 2017), and land use change and
76 associated N fertilisation regimes determine N supply to crops.

77   Figure 1: Inclusion of coupled C-N cycling in the terrestrial biosphere models contributing to the
78   Global Carbon Project, i.e., the TRENDY ensemble.

79

80   The TRENDY ensemble has been extensively evaluated against observations of the C,
81 water, and energy cycles (Collier et al., 2018; Friedlingstein et al., 2022; Seiler et al., 2022).
82 Within the GCP itself, the primary simulated C pools, C fluxes, and water fluxes are evaluated
83 using a skill score system developed by the International Land Model Benchmarking Project
84 (ILAMB) that quantifies model performance by comparing model simulations to observations
85 (Collier et al., 2018; Friedlingstein et al., 2022). ILAMB scores encompass the mean and
86 variability of a given pool or flux over monthly to decadal temporal scales and over grid cell to
87 global spatial scales. However, N cycling has not been explicitly evaluated despite its importance
88 in regulating C cycling. This is in part due to the relatively recent incorporation of N cycling in
89 terrestrial biosphere models (Figure 1) (Fisher and Koven, 2020; Hungate et al., 2003) but also
90 due to the paucity of global observation-based datasets of N cycling: N exists in many forms and
91 is lost from terrestrial ecosystems via numerous pathways (emissions of NH_3, N_2O, NO_x and N_2
92 as well as NO_3^- and NH_4^+ leaching), N processes are generally not measured in situ in networks
93 such as FLUXNET, and remote sensing methodologies for measuring N processes are still in
94 their infancy. Additionally, N processes exhibit extremely high spatial and temporal variabilities
95 and are thus challenging to measure. As such, N cycling has commonly been evaluated by
96 comparing simulated N pools and fluxes to global totals based on a small number of observations
97 that have been scaled up or averaged to yield a value with wide confidence intervals (Davies-
98 Barnard et al., 2020).

99   N cycling is implicitly evaluated by comparing terrestrial biosphere models without N
100 cycling to those with coupled C-N cycling in reproducing observations of the C, water, and
101 energy cycles in the absence of N cycle observations. Results suggest that there are only minor
102 differences between the performance of models with and without N cycling. There is no
103 significant difference between the terrestrial C sink simulated by the TRENDY models with and
104 without N cycling (Friedlingstein et al., 2022) nor between the terrestrial C sink simulated by the
105 models participating in the Multi-scale synthesis and Terrestrial Model Intercomparison Project
106 (MsTMIP) with and without N cycling (Huntzinger et al., 2017). Comparing the mean score
107 across all C, water, and energy cycle variables between TRENDY models with and without N
108 cycling yielded no significant difference (Seiler et al., 2022). However, TRENDY models
109 without N cycling had significantly higher scores for net biome productivity than TRENDY
110 models with N cycling (although all other variables were not significantly different between
111 TRENDY models with and without N cycling, including vegetation C, soil C, net biome
112 productivity, leaf area index, latent heat flux, and runoff, among others) (Seiler et al., 2022).
113 Despite this seeming absence of a difference between models with and without coupled C-N
114 cycling in simulating the current terrestrial C sink, it is imperative that N constraints on C
115 cycling are properly represented by terrestrial biosphere models in order to realistically simulate
116 the terrestrial C sink under future global change, which modifies the C/N balance through N
117 limitation of CO_2 fertilisation and intensifying N deposition among other effects of global
118 change. As such, explicitly evaluating N cycling processes themselves is necessary to assess the
119 ability of terrestrial biosphere models to capture the underlying mechanisms that determine
120 terrestrial C sequestration and thus to realistically project the future terrestrial C sink under
121 global change.

122   Here, we synthesise the N pools and fluxes simulated by 11 terrestrial biosphere models
123 in the TRENDY ensemble that participated in the 2022 GCP. We evaluate their performance in
124 reproducing observations of three key variables of the N cycle: biological N fixation, vegetation
125 C:N ratio, and soil C:N ratio. These three variables are critical to C cycling because (1)
126 biological N fixation is the dominant natural N supply to terrestrial ecosystems, influencing the
127 degree of N limitation of plant growth and thus terrestrial C sequestration, and (2) vegetation and
128 soil C:N ratios reflect assimilated C per unit N and thus terrestrial C storage.

129

130 **2 Methods**

131 **2.1 Simulation Protocol**

132   For the 2022 GCP (version 11), the TRENDY ensemble consisted of 16 terrestrial
133 biosphere models, 11 of which represent N cycling (CABLE-POP, CLM5.0, DLEM, ISAM,
134 JSBACH, JULES-ES, LPJ-GUESS, LPX-Bern, OCNv2, ORCHIDEEv3, and SDGVM).
135 Although SDGVM includes a representation of N cycling, its representation is simplistic and was
136 therefore not included. Additionally, CLASSIC contributed to the 2022 GCP without coupled C-
137 N cycling; the S3 simulation was repeated by CLASSIC with coupled C-N cycling following the
138 2022 GCP protocol and was used here. Overall, we analysed eleven models with coupled C-N
139 cycling (Table 1).

140 Table 1: Terrestrial biosphere models in the TRENDY-N ensemble and descriptions of their
141 representations of N limitation of vegetation growth, biological N fixation, vegetation response
142 to N limitation (i.e., strategies in which vegetation invests C to increase N supply in N-limited
143 conditions), and N limitation of decomposition.

	Reference	N limitation of vegetation growth	Biological N fixation	Vegetation response to N limitation	N limitation of decomposition
CABLE-POP	(Haverd et al., 2018)	V_{cmax} flexible C:N stoichiometry	Time-invariant	Static	N-invariant
CLASSIC	(Melton et al., 2020)	V_{cmax} flexible C:N stoichiometry	f(N limitation of vegetation growth)	Dynamic (biological N fixation)	N-invariant
CLM5.0	(Lawrence et al., 2019)	V_{cmax} flexible C:N stoichiometry	f(N limitation of vegetation growth)	Dynamic (biological N fixation, mycorrhizae, retranslocation)	f(soil N)
DLEM	(Tian et al., 2015)	GPP	f(soil T, soil H_2O, soil C, soil N)	Dynamic (root allocation)	f(soil N)
ISAM	(Shu et al., 2020)	GPP	f(ET)	Static	f(soil N)
JSBACH	(Reick et al., 2021)	NPP	f(NPP)	Static	f(soil N)
JULES-ES	(Wiltshire et al., 2021)	NPP	f(NPP)	Static	f(soil N)
LPJ-GUESS	(Smith et al., 2014)	V_{cmax} flexible C:N stoichiometry	f(ET)	Dynamic (root allocation)	N-invariant
LPX-Bern	(Lienert and Joos, 2018)	NPP	Derived post hoc to simulate a closed N cycle	Static	N-invariant
OCNv2	(Zaehle and Friend, 2010)	V_{cmax} flexible C:N stoichiometry	f(N limitation of vegetation growth)	Dynamic (root allocation)	f(soil N)

ORCHIDEEv3	(Vuichard et al., 2019)	V_{cmax} flexible C:N stoichiometry	Time-invariant	Static	N-invariant

144

145   We analysed the S3 simulation which includes historical changes in atmospheric CO_2,
146   climate, N deposition, N fertilisation, and land use from 1851 to 2021 (see Friedlingstein et al.
147   (2022) for a full description of the simulation protocol). Briefly, models were forced with
148   atmospheric CO_2 from Dlugokencky and Tans (2022), the merged monthly Climate Research
149   Unit (CRU) and 6-hourly Japanese 55-year Reanalysis (JRA-55) dataset or the monthly CRU
150   dataset Harris et al. (2020), N deposition from Hegglin et al. (2016) / Tian et al. (2022), N
151   fertilisation from the global N_2O Model Intercomparison Project (NMIP) (Tian et al., 2018), and
152   land use from the LUH2-GCB2022 (Land-Use Harmonization 2) dataset (Chini et al., 2021;
153   Hurtt et al., 2020; Klein Goldewijk et al., 2017a, b). We interpolated outputs from all models to a
154   common resolution of 1° x 1° using bilinear interpolation.

2.2 Terrestrial biosphere model descriptions

156   The terrestrial biosphere models in the TRENDY ensemble employ a wide variety of
157   assumptions and formulations of N cycling processes, reflecting knowledge gaps and divergent
158   theories (Table 1). Here we describe four fundamental aspects of N cycling for each terrestrial
159   biosphere model: N limitation of vegetation growth, biological N fixation, the response of
160   vegetation to N limitation (i.e., strategies in which vegetation invests C to increase N supply in
161   N-limited conditions), and N limitation of decomposition. These have been identified as
162   important challenges for representing N cycling in terrestrial biosphere models (Meyerholt et al.,
163   2020; Peng et al., 2020; Stocker et al., 2016; Wieder et al., 2015a; Zaehle et al., 2015; Zaehle and
164   Dalmonech, 2011).

165   Terrestrial biosphere models differ in how N limitation of vegetation growth is
166   represented (Thomas et al., 2015). Some TRENDY models represent flexible C:N stoichiometry
167   and modelled maximum carboxylation rate of photosynthesis (V_{cmax}) decreases with decreasing
168   leaf N (CABLE-POP, CLASSIC, CLM5.0, LPJ-GUESS, OCNv2, ORCHIDEEv3) following
169   empirical evidence (Walker et al., 2014). Other TRENDY models represent time-invariant C:N
170   stoichiometry and modelled GPP or NPP decreases with N limitation (DLEM, ISAM, JSBACH,
171   JULES-ES, and LPX-Bern). Importantly, flexible vs. time-invariant C:N stoichiometry
172   determines terrestrial C storage per unit N.

173   Biological N fixation is the dominant natural N supply to terrestrial ecosystems (Vitousek
174   et al., 2013). In terrestrial biosphere models, biological N fixation has generally been represented
175   phenomenologically as a function of either net primary productivity (NPP) or evapotranspiration
176   (ET) (Cleveland et al., 1999). More recently, representations of biological N fixation have been
177   updated such that it is up-regulated in N-limited conditions following empirical evidence (Menge
178   et al., 2015; Vitousek et al., 2013; Zheng et al., 2019). The majority of TRENDY models
179   represent biological N fixation phenomenologically (ISAM, JSBACH, JULES-ES, and LPJ-
180   GUESS). Three TRENDY models (CLASSIC, CLM5.0, and OCNv2) represent biological N
181   fixation mechanistically such that it increases with N limitation of vegetation (Kou-Giesbrecht
182   and Arora, 2022; Lawrence et al., 2019; Meyerholt et al., 2016). These representations separate
183   free-living biological N fixation (via soil microbes, epiphytic microbes, lichens, bryophytes, etc.
184   (Reed et al., 2011)) from symbiotic biological N fixation, which is regulated by N limitation of
185   vegetation. DLEM derives biological N fixation as a function of soil temperature, soil moisture,

186 soil C, and soil N. LPX-Bern derives biological N fixation post hoc to simulate a closed N cycle,
187 implicitly including rock N sources (Joos et al., 2020). Finally, CABLE-POP and ORCHIDEEv3
188 represent biological N fixation as a specified time-invariant input over the historical period.
189 Importantly, representing the regulation of biological N fixation by N limitation does not only
190 determine biological N fixation itself but also modulates terrestrial C sequestration: it enables
191 vegetation to increase N uptake in N-limited conditions, reduce N limitation, and thus sustain
192 terrestrial C sequestration. Some TRENDY models (DLEM, LPJ-GUESS, and OCNv2) also
193 represent increasing C allocation to roots with increasing N limitation (Smith et al., 2014; Zaehle
194 and Friend, 2010) following empirical evidence (Poorter et al., 2012). This enables vegetation to
195 increase root N uptake in N-limited conditions, reduce N limitation, and thus sustain terrestrial C
196 sequestration. The response of vegetation to N limitation, which could also include increased C
197 allocation to mycorrhizae (Phillips et al., 2013) (represented in CLM5.0) or increased
198 retranslocation of N during tissue turnover (Du et al., 2020; Han et al., 2013; Kobe et al., 2005)
199 (represented in CLM5.0) is important for determining terrestrial C sequestration.

200 Decomposition rate is controlled by soil temperature, soil moisture, and N content in
201 litter, where increasing litter C:N ratio decreases decomposition rate (Cotrufo et al., 2013). Some
202 TRENDY models represent this reduction in decomposition rate with increasing litter C:N ratio
203 (CLM5.0, DLEM, ISAM, JSBACH, JULES-ES, and OCNv2) following empirical evidence.

204 **2.3 Observation-based datasets**

205 We interpolated observation-based datasets to a common resolution of 1° x 1° using
206 bilinear interpolation for comparison against model outputs. To compare model outputs against
207 observation-based datasets we averaged model outputs over 1980–2021, which spans the period
208 in which most measurements were made.

209 **2.3.1 Biological N fixation**

210 A biological N fixation observation-based dataset was derived from Davies-Barnard and
211 Friedlingstein (2020), a global meta-analysis of field measurements of natural biological N
212 fixation (free-living and symbiotic) that scales biome-specific means onto the Collection 5
213 MODIS Global Land Cover Type International Geosphere-Biosphere Programme (IGBP)
214 product (Friedl et al., 2010). To account for agricultural biological N fixation, we assumed that
215 N-fixing crops account for 15.7% of global cropland area (U.S. Department of Agriculture,
216 2022) and their biological N fixation rate as 11.5 g N m^{-2} yr^{-1} (Herridge et al., 2008). We
217 assumed that N-fixing crops are distributed evenly across all cropland. We amended the dataset
218 from Davies-Barnard and Friedlingstein (2020) to include agricultural biological N fixation
219 (DBF-USDA).

220 The score of LPX-Bern in simulating biological N fixation is not analysed because it
221 implicitly includes rock N sources and is thus not directly comparable to the observation-based
222 dataset.

223 **2.3.2 Vegetation C:N ratio**

224   A vegetation C:N ratio observation-based dataset was derived by scaling biome-specific
225 means from the TRY plant trait database (Kattge et al., 2020) onto the Collection 5 MODIS
226 Global Land Cover Type IGBP product (Friedl et al., 2010). First, we obtained N content per dry
227 mass for leaves, root, and stem, as well as C content per dry mass for leaves, root, and stem from
228 the TRY plant trait database. We selected entries that reported species. Second, we obtained
229 plant functional type (PFT) for each species from the TRY plant trait database. We categorised
230 each PFT into the IGBP land cover types (Table A1) and then used this to categorise each entry
231 into the IGBP land cover types. We averaged across entries in each IGBP land cover type. Third,
232 we divided mean tissue C content per tissue dry mass by mean tissue N content per tissue dry
233 mass for each tissue and for each IGBP land cover type. Fourth, we weighed each tissue by its
234 PFT-specific fraction of total biomass from Poorter et al. (2012) to obtain total vegetation C:N
235 ratio for each IGBP land cover type. Lastly, we scaled total vegetation C:N ratio for each IGBP
236 land cover type to the Collection 5 MODIS Global Land Cover Type IGBP product.

237 2.3.3 Soil C:N ratio

238   A soil C:N ratio observation-based dataset was derived from soil C and soil N products
239 from SoilGrids (Poggio et al., 2021), which provides globally gridded datasets of soil organic C
240 and total soil N at a 250m x 250m resolution for six layers up to a depth of 200 cm. These
241 estimates are derived using machine learning methods and soil observations from 240 000
242 locations across the globe and over 400 environmental covariates. We summed soil C over all
243 layers and soil N over all layers (using the bulk density and depth of each layer) then obtained
244 the soil C:N ratio.

245 2.3.4 C cycling variables

246   In addition to evaluating N cycling variables, we also evaluated the primary C cycling
247 variables: gross primary productivity (GPP), net biome productivity (NBP), vegetation C
248 (CVEG), soil C (CSOIL), and leaf area index (LAI). These variables have been previously
249 evaluated in detail for the terrestrial biosphere models in the TRENDY ensemble (GCP 2021) in
250 Seiler et al. (2022). Seiler et al. (2022) gives further details on the observation-based datasets
251 used to evaluate the primary C cycling variables. Briefly, we evaluated GPP against MODIS
252 (Zhang et al., 2017), GOSIF (Li and Xiao, 2019), and FLUXCOM (Jung et al., 2020) products.
253 We evaluated NBP against the CAMS (Agustí-Panareda et al., 2019), CarboScope (Rödenbeck
254 et al., 2018), and CT2019 (Jacobson et al., 2020) products. We evaluated CVEG against the
255 GEOCARBON (Avitabile et al., 2016; Santoro et al., 2015), Zhang and Liang (2020), and Huang
256 et al. (2021) products. We evaluated LAI against AVHRR (Claverie et al., 2016), Copernicus
257 (Verger et al., 2014), and MODIS (Myneni et al., 2002) products. We evaluated CSOIL against
258 HWSD (Todd-Brown et al., 2013; Wieder, 2014) and SoilGrids (Hengl et al., 2017) products.
259 These observation-based products are globally gridded.

260 2.4 Model evaluation with the Automated Model Benchmarking R Package (AMBER)

261   The Automated Model Benchmarking R (AMBER) package developed by Seiler et al.
262 (2021) quantifies model performance in reproducing observation-based datasets using a skill
263 score system that is based on ILAMB (Collier et al., 2018). Five scores assess the simulated

264   time-mean bias (S_{bias}), monthly centralised root-mean-square-error (S_{rmse}), seasonality (S_{phase}),
265   inter-annual variability (S_{iav}), and spatial distribution (S_{dist}) in comparison to the observation-
266   based dataset. Scores are dimensionless and range from 0 to 1, where higher values indicate
267   better model performance. The overall score for each variable ($S_{overall}$) is

268    $$S_{overall} = \text{mean}\big(S_{bias}, S_{rmse}, S_{phase}, S_{iav}, S_{dist}\big)$$

269   We calculated the overall score for each C and N cycling variable. Because biological N fixation,
270   vegetation C:N ratio, and soil C:N ratio datasets are representative of the present-day (as a single
271   time point), S_{rmse}, S_{phase}, and S_{iav} are not defined and thus do not contribute to $S_{overall}$. This also
272   holds for vegetation C and soil C. The calculation of each score is described in detail in Seiler et
273   al. (2022).

274   2.5 Statistics

275   We used a Mann-Kendall trend test to assess the existence of a statistically significant
276   trend in the time series over the historical period for simulated C and N cycling variables (Hipel
277   and McLeod, 1994). We calculated Spearman's rank correlation coefficient to assess the
278   existence of statistically significant correlations between overall scores, present-day global
279   values, and Kendall's tau. We used a t-test or ANOVA (p-value < 0.05) to assess the existence of
280   statistically significant differences between overall scores, present-day global values, and
281   Kendall's tau for models with different representations of N limitation of vegetation growth,
282   biological N fixation, vegetation response to N limitation, and N limitation of decomposition
283   (Table 1).

284

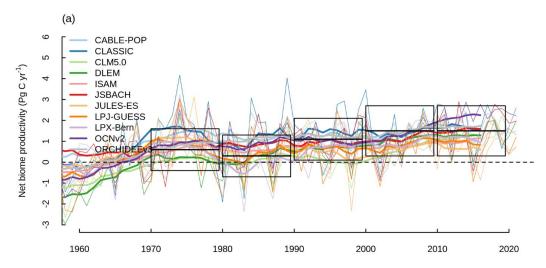### 285   3 Results

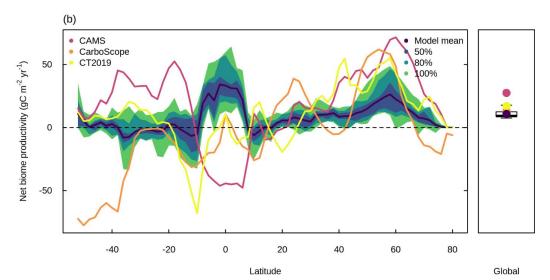### 286   3.1 Net biome productivity

287   Figure 2 shows NBP simulated by the TRENDY ensemble models with coupled C-N
288   cycling (hereafter referred to as the TRENDY-N ensemble). NBP is the difference between the
289   net natural atmosphere-land flux of CO_2 and land use change CO_2 emissions. Positive values of
290   NBP indicate a terrestrial C sink whereas negative values of NBP indicate a terrestrial C source.
291   All TRENDY-N ensemble models suggest a terrestrial C sink for the present-day, agreeing with
292   the global C budget constraint from the 2022 Global C Budget with most models within two
293   standard deviations of the mean (1.5 ± 0.6 Pg C for 2012–2021) (Figure 2a). The TRENDY-N
294   ensemble agrees reasonably well with observations globally, agreeing somewhat better with
295   CarboScope and CT2019 than with CAMS (Figure 2b). However, the latitudinal distributions of
296   the observation-based datasets display weak agreement among themselves, with opposing signs
297   in multiple regions, especially at southern latitudes and at high northern latitudes (Figure 2b).
298   This is in part due to the smaller land area at these latitudes. The region showing the strongest
299   agreement is mid to high northern latitudes, in which both the TRENDY-N ensemble and
300   observations suggest a terrestrial C sink (Figure 2b).

Figure 2: Net biome productivity (NBP) simulated by the TRENDY-N ensemble. a. Global NBP
from 1960 to 2021. The boxes indicate the global C budget constraint (difference between fossil
fuel CO_2 emissions and the growth rate of atmospheric CO_2 and the uptake of CO_2 by oceans;
mean ± 2 standard deviation) from the 2022 Global C Budget (Friedlingstein et al., 2022). Thick
lines indicate the moving average over 10 years and thin lines indicate the annual time series. b.
Latitudinal distribution and global mean of NBP (averaged over 1980–2021) in comparison to
three datasets (CAMS (Agustí-Panareda et al., 2019), CarboScope (Rödenbeck et al., 2018), and
CT2019 (Jacobson et al., 2020)). The boxplot shows the median, interquartile range (box), and
80% percentiles (whiskers) of the global mean of NBP.

3.2 Overview of N cycling

Figure 3 shows a schematic of the N cycle alongside the primary N fluxes and C:N ratios of the primary pools simulated by the TRENDY-N ensemble for the present-day (averaged over 1980–2021) as well as observation-based estimates for these variables that have previously been used for model evaluation (Davies-Barnard et al., 2020). Simulated biological N fixation ranged between 20 and 566 Tg N yr^{-1} (Table 2) in comparison to the observation-based estimate of 148 Tg N yr^{-1}, which includes both natural biological N fixation (88 Tg N yr^{-1} (52 – 130 Tg N yr^{-1}) (Davies-Barnard and Friedlingstein, 2020)) and agricultural biological N fixation (50 – 70 Tg N yr^{-1} (Herridge et al., 2008)). Simulated N_2O emissions ranged between 0.9 and 11.0 Tg N yr^{-1} (Table 2) in comparison to the observation-based estimate of 10.8 Tg N yr^{-1} (7.1 – 16.0 Tg N yr^{-1}) (Tian et al., 2020). Simulated N losses (which include emissions of NH_3, N_2O, NO_x and N_2 as well as NO_3^- and NH_4^+ leaching) ranged between 87 and 603 Tg N yr^{-1} (Table 2) in comparison to the observation-based estimate of 293 Tg N yr^{-1} (Fowler et al., 2013). The simulated vegetation C:N ratio ranged between 103 and 222 (Table 2) in comparison to the observation-based estimate of 133 (Zechmeister-Boltenstern et al., 2015). The simulated combined litter-soil C:N ratio ranged between 10 and 64 (Table 2) in comparison to the observation-based estimate of 15 (Zechmeister-Boltenstern et al., 2015). Biological N fixation has the largest inter-model spread with a coefficient of variation of 1.06 (Table 2). Figure 4 shows the geographical distribution of the primary N pools and fluxes simulated by the TRENDY-N ensemble for the present-day (averaged over 1980–2021).
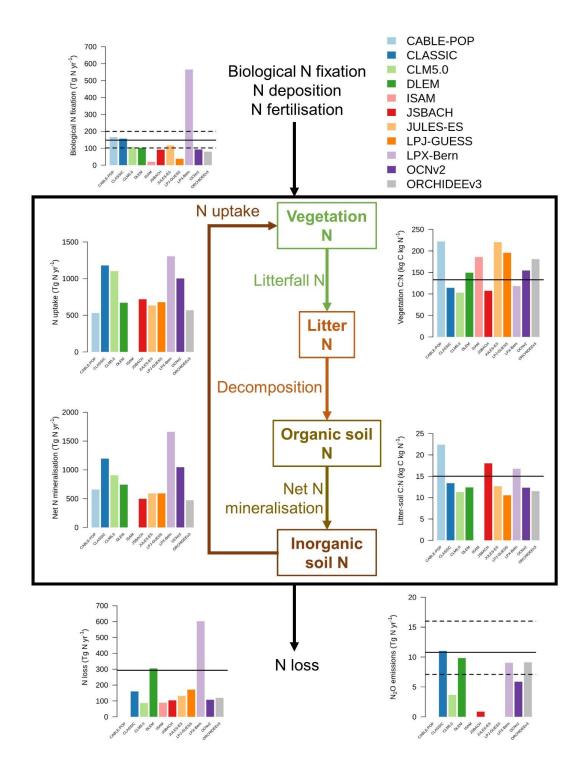
Figure 3: The N cycle and the primary N pools and fluxes simulated by the TRENDY-N ensemble (averaged over 1980–2021). Horizontal black lines indicate observation-based estimates that have previously been used for model evaluation (biological N fixation from Davies-Barnard and Friedlingstein (2020) and Herridge et al. (2008), vegetation and combined litter-soil C:N ratios from Zechmeister-Boltenstern et al. (2015), N_2O emissions from Tian et al. (2020), and N losses from Fowler et al. (2013)). The black box indicates the terrestrial biosphere. N enters the terrestrial biosphere via biological N fixation, N deposition, and N fertilisation (entering the organic soil N pool, the inorganic soil N pool (ammonium (NH_4^+) or nitrate (NO_3^-)), or the vegetation N pool). N is transferred from the inorganic soil N pool to the vegetation N pool via N uptake. N is transferred from the vegetation N pool to the litter N pool via N litterfall. N is transferred from the litter N pool to the organic soil N pool via decomposition. N is transferred from the organic soil N pool to the inorganic soil N pool via net N mineralisation. N exits the terrestrial biosphere via N loss (which includes N leaching from soils and N_2O, NO_x, NH_3, and N_2 emissions from both soils and land use change). Not all models provide output for each N pool or flux. Note that biological N fixation simulated by LPX-Bern implicitly includes rock N sources.

Figure 4: Geographical distributions of a. vegetation N, b. litter N, c. soil N, d. biological N
fixation, e. N uptake, f. net N mineralisation, g. N$_2$O emissions, and h. N loss simulated by the
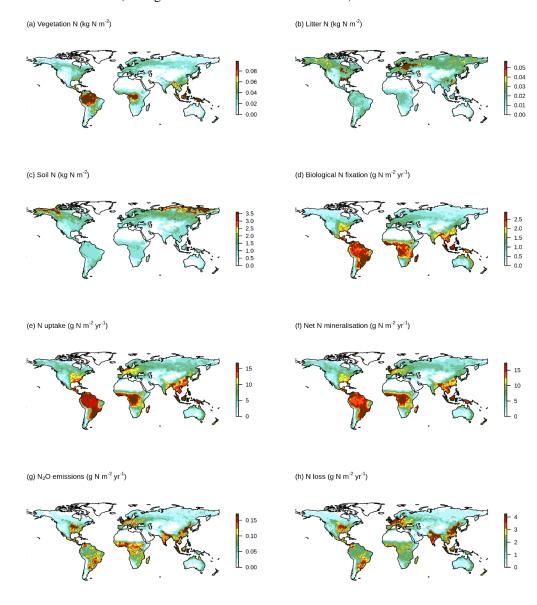TRENDY-N ensemble (averaged across models over 1980–2021).

(a) Vegetation N (kg N m^{-2})

(b) Litter N (kg N m^{-2})

(c) Soil N (kg N m^{-2})

(d) Biological N fixation (g N m^{-2} yr^{-1})

(e) N uptake (g N m^{-2} yr^{-1})

(f) Net N mineralisation (g N m^{-2} yr^{-1})

(g) N$_2$O emissions (g N m^{-2} yr^{-1})

(h) N loss (g N m^{-2} yr^{-1})

352   Table 2: Global mean and coefficient of variation of each N pool and flux simulated by the
353   TRENDY-N ensemble (across models over 1980–2021).

	Coefficient of variation	Global mean	Global median	Global minimum	Global maximum
Vegetation N (Tg N)	0.41	2.94	2.94	1.50	5.58
Litter N (Tg N)	0.81	1.94	1.08	0.73	5.61
Soil N (Tg N)	0.67	101.43	81.21	32.10	277.41
Biological N fixation (Tg N yr^{-1})	1.06	139.63	101.83	19.92	565.53
N uptake (Tg N yr^{-1})	0.33	838.78	698.11	529.53	1304.87
Net N mineralisation (Tg N yr^{-1})	0.45	836.00	700.28	471.39	1661.53
N$_2$O emissions (Tg N yr^{-1})	0.53	7.06	9.04	0.86	11.01
N loss (Tg N yr^{-1})	0.85	187.62	125.96	87.02	602.77
Vegetation C:N ratio	0.28	159.28	154.50	102.84	222.22
Soil C:N ratio	0.90	17.32	11.13	10.00	63.57

354

355   Figure 5 shows the time series of the change from pre-industrial levels of the primary N
356 pools and fluxes from 1850 to 2021 simulated by the TRENDY-N ensemble. Figure 6 shows the
357 corresponding Kendall's tau which identifies the existence of a statistically significant trend
358 (Table A2). Some models suggest decreasing vegetation N (6/11 models), whereas other models
359 suggest increasing vegetation N (2/11 models) or no trend in vegetation N (3/11 models). Some
360 models suggest decreasing soil N (7/11 models), whereas other models suggest increasing soil N
361 (4/11 models). Some models suggest increasing biological N fixation (7/11 models), whereas
362 other models suggest decreasing biological N fixation (2/11 models) or no trend in biological N
363 fixation (2/11 models). All models suggest increasing N uptake (10/10 models). Most models
364 suggest increasing net N mineralisation rate (9/10 models) or no trend in N mineralisation rate
365 (1/10 models). All models suggest increasing N_2O emissions (7/7 models) and increasing N loss
366 (10/10 models).

Figure 5: Time series of the change from the pre-industrial level (averaged over 1850–1870) of a.
vegetation N, b. litter N, c. soil N, d. biological N fixation, e. N uptake, f. net N mineralisation,
g. N_2O emissions, and h. N loss simulated by the TRENDY-N ensemble from 1850 to 2021.
Figure A4 shows the time series for each N pool and N flux simulated by the TRENDY-N
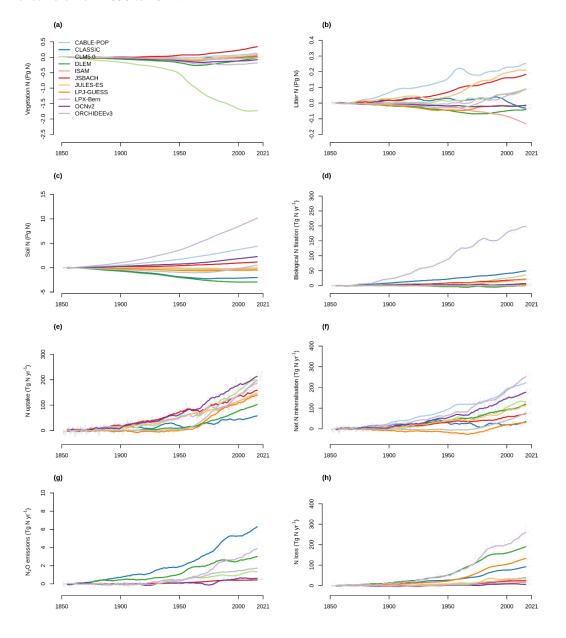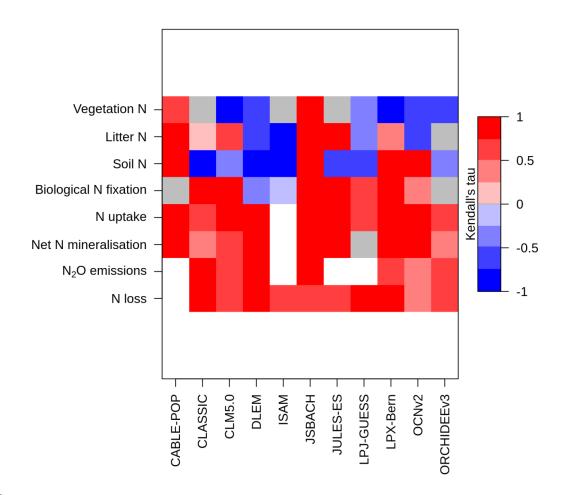ensemble from 1850 to 2021.

373 Figure 6: Kendall's tau from the Mann-Kendall test (p-value < 0.05) for each N pool and N flux
374 time series simulated by the TRENDY-N ensemble from 1850 to 2021 (Table A2). A positive
375 value (red) indicates an increasing trend and a negative value (blue) indicates a decreasing trend
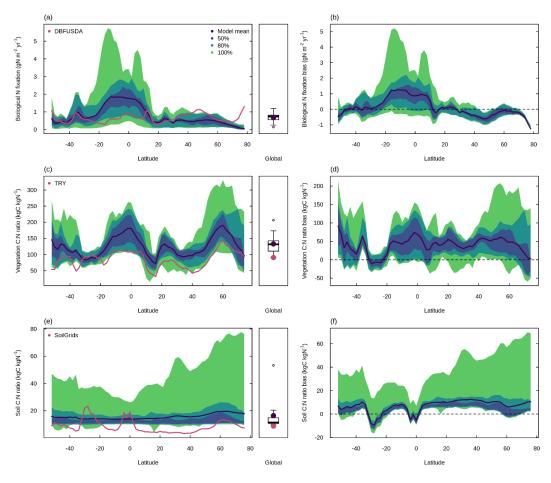376 Gray indicates a statistically insignificant value and white indicates a missing value.

377

3.3 Evaluation of biological N fixation, vegetation C:N ratio, and soil C:N ratio

In comparison to the observation-based dataset from Davies-Barnard and Friedlingstein (2020) and the U.S. Department of Agriculture (USDA), the TRENDY-N ensemble reproduced global biological N fixation (101.8 Tg N yr^{-1} vs. 108.0 Tg N yr^{-1}; Figure 7a and Table 2) but overestimated low-latitude biological N fixation and underestimated high-latitude biological N fixation in the Northern hemisphere (Figure 7b). In comparison to the observation-based dataset from the TRY plant trait database, the TRENDY-N ensemble overestimated the global vegetation C:N ratio (154.5 vs. 90.5; Figure 7c and Table 2) and overestimated the vegetation C:N ratio across latitudes while capturing its latitudinal pattern (Figure 7d). In comparison to the observation-based dataset from SoilGrids, the TRENDY-N ensemble overestimated the global soil C:N ratio, simulating a relatively constant soil C:N ratio across latitudes (11.1 vs. 8.8; Figure 7e and Table 2). The TRENDY-N ensemble was thus unable to capture the latitudinal pattern of the soil C:N ratio (Figure 7f).

Figure 7: Latitudinal distributions and global means of biological N fixation, vegetation C:N ratio, and soil C:N ratio simulated by the TRENDY-N ensemble (averaged across models over 1980–2021) in comparison to observations. ace. show the latitudinal distribution of the mean and boxplots show the global mean. bdf. show the latitudinal distribution of the bias. Latitudinal distributions show the mean (black line) and the 50%, 80%, and 100% percentiles across models. Boxplots show the median, interquartile range (box), and 80% percentiles (whiskers) across models. Observation-based datasets are from Davies-Barnard and Friedlingstein (2020) and the U.S. Department of Agriculture (USDA) for biological N fixation, the TRY plant trait database for vegetation C:N ratio, and SoilGrids for soil C:N ratio. LPX-Bern simulations are not shown in ab. Latitudinal distributions and global means of individual models in the TRENDY-N ensemble are shown in Figure A5.
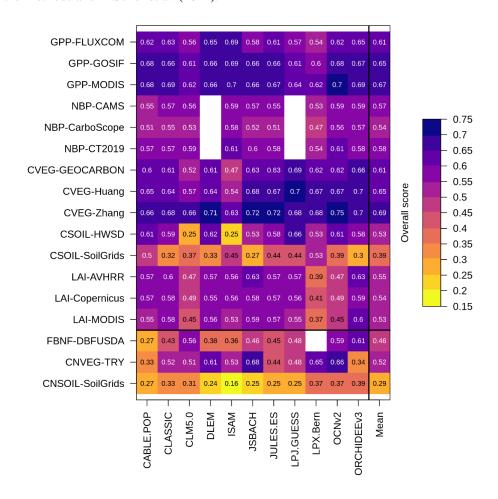
403   The overall score is a metric of model performance in reproducing an observation-based
404   dataset. Overall scores for biological N fixation, vegetation C:N ratio, and soil C:N ratio (0.46,
405   0.52, and 0.29 averaged across models, respectively) were lower than those for C cycling
406   variables (0.58 averaged across all C cycling variables and across models) (Figure 8). The mean
407   overall score for vegetation C:N ratio across models (0.52) was lower than the mean overall
408   scores for vegetation C across models (which ranged from 0.61 to 0.69 depending on the
409   observation-based dataset used to derive the score). Similarly, the mean overall score for soil
410   C:N ratio across models (0.20) was lower than the mean overall scores for soil C across models
411   (which ranged from 0.39 to 0.53 depending on the observation-based dataset used to derive the
412   score). Overall scores varied between 0.27 and 0.61 for biological N fixation, between 0.33 and
413   0.68 for vegetation C:N ratio, and between 0.16 and 0.39 for soil C:N ratio.

Figure 8: Overall scores of the TRENDY-N ensemble in simulating C and N cycling variables:
gross primary productivity (GPP), net biome productivity (NBP), vegetation C (CVEG), soil C
(CSOIL), leaf area index (LAI), biological N fixation (FBNF), vegetation C:N ratio (CNVEG),
and soil C:N ratio (CNSOIL). Abbreviations of the observation-based datasets are described in
the Methods and in Seiler et al. (2022).

420   For N cycling variables, the overall score is composed of the time-mean bias score
421   (which assesses the difference between the time-mean of model simulations and the time-mean
422   of the observation-based dataset) and the spatial distribution score (which assesses the ability of
423   the model to reproduce the spatial pattern of the observation-based dataset) (Collier et al., 2018;
424   Seiler et al., 2022). For biological N fixation, the time-mean bias score averaged across models
425   was 0.50 and the mean spatial distribution score across models was 0.41 (Table A3). For the
426   vegetation C:N ratio, the time-mean bias averaged score across models was 0.47 and the mean
427   spatial distribution score across models was 0.58 (Table A3). For the soil C:N ratio, the time-
428   mean bias score averaged across models was 0.39 and the mean spatial distribution score across
429   models was 0.19 (Table A3).

430   Note that, for C fluxes, the overall score is composed of not only the time-mean bias
431   score and the spatial distribution score, but also the monthly centralised root-mean-square-error
432   score (which assesses the ability of the model to reproduce the time series of the observation-
433   based dataset), the seasonality score (which assess the ability of the model to reproduce the
434   seasonality of the observation-based dataset), and the inter-annual variability score (which
435   assesses the ability of the model to reproduce the inter-annual variability of the observation-
436   based dataset) because observation-based datasets of C fluxes are available over time (whereas
437   observation-based datasets of C pools and all N cycling variables are representative of the
438   present-day (as a single time point)).

3.4 Representation of N cycling processes

440   There were no statistically significant differences in overall scores between models with
441   different representations of N limitation of vegetation growth (decreasing V_{cmax} and flexible C:N
442   stoichiometry vs. decreasing NPP), different representations of biological N fixation (function of
443   N limitation of vegetation growth vs. function of NPP or ET vs. time-invariant), different
444   representations of the response of vegetation to N limitation (dynamic vs. static), or different
445   representations of N limitation of decomposition (function of soil N vs. N-invariant) (Table A4).
446   However, models that represented decomposition as a function of soil N had a significantly
447   higher NBP score (corresponding to CT2019) than models that represented decomposition as N-
448   invariant. Similarly, there were no statistically significant differences between present-day global
449   values or Kendall's tau of primary C and N pools and fluxes between models with different
450   representations of N limitation of vegetation growth, biological N fixation, vegetation response
451   to N limitation, and N limitation of decomposition (Table A5 and A6). Figure A1 shows
452   correlations between present-day global values of the primary C and N pools and fluxes across
453   the TRENDY-N ensemble. Figure A2 shows correlations between Kendall's tau of the primary C
454   and N pools and fluxes across the TRENDY-N ensemble. Figure A3 shows correlations between
455   overall scores of the primary C and N pools and fluxes across the TRENDY-N ensemble.

456

4 Discussion

458   Despite the pivotal importance of N in constraining terrestrial C cycling and ultimately
459   the terrestrial C sink, there is substantial variation in simulated N cycling processes by the

460 terrestrial biosphere models in the TRENDY-N ensemble. The magnitude of N pools and fluxes
461 differ considerably between models, between 19.9 and 565.5 Tg N yr^{-1} for biological N fixation
462 (CV = 1.1), between 1.5 and 5.6 Tg N for vegetation N (CV = 0.4), between 32.1 and 277.4 Tg
463 N for soil N (CV = 0.7), and between 87.0 and 602.8 Tg N yr^{-1} for N loss (CV = 0.9). The spread
464 across the TRENDY-N ensemble suggests that approaches to represent N cycling processes vary
465 among terrestrial biosphere models and that there is no clear consensus yet on what the best
466 approaches are, supporting the use of an ensemble approach to capture the uncertainties in our
467 understanding of the N cycle, similarly to the C cycle (Tebaldi and Knutti, 2007).

468 Additionally, the historical trajectories of the N pools and fluxes differ between models:
469 some models simulate increasing vegetation N and soil N whereas others simulate decreasing
470 vegetation N and soil N between 1850 and 2021. These are the result of a host of interacting
471 global change drivers (CO$_2$ fertilisation, intensifying N deposition, rising temperature and
472 varying precipitation, land use change and associated N fertilisation regimes) whose effects are
473 challenging to disentangle without additional simulations. For example, while intensifying N
474 deposition and N fertiliser use could drive increasing soil N and N uptake, land use change could
475 increase N losses from both vegetation N and soil N. Despite these large differences across
476 models in the historical trajectories of vegetation N and soil N, all models simulate the historical
477 terrestrial C sink in line with observations. This suggests that the underlying N cycling processes
478 that regulate terrestrial C sequestration operate differently across models and may not be fully
479 captured. Modelled experimental manipulations (such as CO$_2$ fertilisation or N fertilisation
480 experiments) are imperative to evaluate model formulations of the underlying mechanisms of C-
481 N cycling interactions given that it is these processes that dictate the response of terrestrial C
482 sequestration to global change (Medlyn et al., 2015; Wieder et al., 2019; Zaehle et al., 2014).

483 Most models suggest increasing biological N fixation between 1850 and 2021. This
484 occurs either as a result of increasing vegetation biomass or the up-regulation of biological N
485 fixation due to N limitation imposed by CO$_2$ fertilisation or a combination thereof, depending on
486 the representation of biological N fixation in a given model (Table 1). This follows observations
487 that suggest that biological N fixation is stimulated by CO$_2$ fertilisation (Zheng et al., 2020),
488 although its mechanism (i.e., up-regulated biological N fixation in N-limited conditions) may not
489 be captured. Similarly, most models also suggest increasing N uptake between 1850 and 2021.
490 This also occurs as a result of increasing vegetation biomass, increasing soil N from intensifying
491 N deposition and N fertiliser use, or increasing biological N fixation, mycorrhizae and root
492 allocation due to N limitation imposed by CO$_2$ fertilisation, again dependent on the
493 representation of the vegetation response to N limitation in a given model (Table 1). Most
494 models suggest increasing net N mineralisation rate between 1850 and 2021 likely due to rising
495 temperature following observations (Liu et al., 2017). Most models suggest increasing N$_2$O
496 emissions (and N losses) between 1850 and 2021 likely due to rising temperature and
497 intensifying N deposition and N fertiliser use following observations (Tian et al., 2020).

498 We focused on three key N cycling processes for evaluation: biological N fixation,
499 vegetation C:N ratio, and soil C:N ratio. These three key N cycling processes have important
500 implications for projecting the future terrestrial C sink. Biological N fixation is the dominant

501   natural N supply to terrestrial ecosystems and allows vegetation to increase N uptake in N-
502   limited conditions, reduce N limitation, and thus sustain terrestrial C sequestration, such as in
503   response to N limitation imposed by CO_2 fertilisation (Zheng et al., 2020). Vegetation and soil
504   C:N ratios reflect assimilated C per unit N and thus terrestrial C sequestration. They can
505   potentially vary, such as in response to high photosynthesis rates relative to N uptake rates driven
506   by CO_2 fertilisation (Elser et al., 2010). Overall scores of N cycling variables, which quantify
507   model performance in reproducing an observation-based dataset, are lower than overall scores of
508   corresponding C cycling variables, suggesting that models could be less capable of capturing N
509   cycling processes than C cycling processes. However, this could also be due to the significant
510   uncertainty associated with measurements of N cycling processes as discussed below. Besides
511   models that represent N limitation of decomposition yielding a higher overall NBP score, there
512   were no statistically significant differences between models with different representations of N
513   limitation of vegetation growth, biological N fixation, the response of vegetation to N limitation,
514   and N limitation of decomposition for the overall score, present-day global value, or Kendall's
515   tau. This is likely due to the low number of models in the TRENDY-N ensemble and the
516   confounding influence of other process representations. Studies have explored the validity of
517   different representations of N cycling processes within a single model, suggesting that alternative
518   representations of a biological N fixation, ecosystem C:N stoichiometry, and ecosystem N losses
519   lead to substantial differences in simulated C cycling (Kou-Giesbrecht and Arora, 2022;
520   Meyerholt et al., 2020; Peng et al., 2020; Wieder et al., 2015a).

521   The TRENDY-N ensemble reproduced global observation-based biological N fixation
522   but tended to overestimate low-latitude biological N fixation and underestimate high-latitude
523   biological N fixation. This is likely because most models represented biological N fixation
524   phenomenologically as a function of a measure of vegetation activity (either NPP or ET). Since
525   there is higher vegetation activity at low latitudes than at high latitudes these models thus
526   represent higher biological N fixation at low latitudes than at high latitudes. However, because
527   biological N fixation is down-regulated in non-N-limited conditions, it is often down-regulated at
528   low latitudes, which are generally not (or at least less) N-limited (Barron et al., 2011; Batterman
529   et al., 2013; Sullivan et al., 2014). While CLASSIC, CLM5.0, and OCNv2 can represent the
530   down-regulation of biological N fixation in non-N-limited conditions, they still simulate high
531   low-latitude biological N fixation. This suggests that the strength of regulation of biological N
532   fixation could be insufficient and/or that there could be unaccounted N sources at low latitudes.
533   For example, rock N weathering could be a significant N source to terrestrial ecosystems. Some
534   estimates have suggested that rock N weathering could be as high as $11 - 18$ Tg N yr^{-1} globally
535   (Houlton et al., 2018) but is not explicitly represented in the TRENDY-N ensemble (with the
536   exception of LPX-Bern which calculates all external N sources post hoc to simulate a closed N
537   cycle thereby implicitly including rock N sources). The discrepancy between modelled and
538   observed biological N fixation could also be due to uncertainty in the observation-based dataset
539   given the difficulties associated with measuring biological N fixation (Soper et al., 2021).
540   Ecological theory (Hedin et al., 2009) has suggested that natural biological N fixation should be
541   higher at low latitudes given large N losses, in contrast to the observation-based dataset from
542   Davies-Barnard and Friedlingstein (2020). Observational uncertainty is discussed further below.

543   The TRENDY-N ensemble overestimated global observation-based vegetation C:N ratio
544 but reproduced its latitudinal pattern (as also indicated by its higher spatial distribution score).
545 This is because most models represent different plant functional types (e.g., evergreen needleleaf
546 trees, deciduous broadleaf trees, evergreen broadleaf trees, etc.) with different tissue C:N ratios
547 (which can either be flexible within a constrained range or time-invariant). These plant
548 functional types are geographically distributed according to similar land cover products. The
549 TRENDY-N ensemble overestimated global observation-based soil C:N ratio and failed to
550 reproduce its latitudinal pattern (as also indicated by its lower spatial distribution score). In
551 particular, models failed to reproduce the peak at the equator and the peak at approximately -
552 30°S, corresponding to tropical forests and deserts respectively. This is because most models
553 represent a constant soil C:N ratio (both temporally and spatially) and are thus unable to capture
554 the spatial variability in the soil C:N ratio. Improving the representation of soil N is an important
555 future direction for terrestrial biosphere model development given the essential feedbacks
556 between soil N and soil C.

557   Evaluating N cycling in terrestrial biosphere models is severely restricted by the lack of
558 available observations of N cycling. N cycling processes are notoriously difficult to measure,
559 such as biological N fixation (Soper et al., 2021) and gaseous N losses (Barton et al., 2015). In
560 the past, N cycling has been commonly evaluated by comparison to estimates of global N pools
561 and fluxes derived from a small number of observations that have been scaled up or averaged to
562 yield a value with wide confidence intervals (Davies-Barnard et al., 2020). Not only are these
563 global totals highly uncertain, but they also do not allow for the analysis of spatial patterns. Here,
564 we present an improved framework to evaluate three key N cycling processes – biological N
565 fixation, vegetation C:N ratio, and soil C:N ratio – in terrestrial biosphere models. However,
566 these globally-gridded observation-based datasets are also uncertain, given uncertainty in the
567 estimates of tissue C:N ratios for different plant functional types and tissue fraction of total
568 biomass (especially those of roots and wood which had a lower number of measurements in
569 comparison to that of leaves), as well as in the measurements and models used to derive soil N
570 (Batjes et al., 2020). Importantly, more observations of additional N cycling processes are
571 necessary to fully evaluate N cycling in terrestrial biosphere models. Multiple observation-based
572 datasets from different sources of a given N cycling process are necessary to evaluate
573 observational uncertainty (Seiler et al., 2021). Observation-based datasets of N cycling processes
574 at intra-annual and inter-annual time scales are necessary to assess temporal patterns.
575 Paleoclimatic observations could also be utilised for evaluation (Joos et al., 2020). Leveraging
576 advances in remote sensing (Knyazikhin et al., 2013; Townsend et al., 2013) as well as
577 incorporating N cycling process measurements into research networks such as FLUXNET (Vicca
578 et al., 2018) is essential.

579   While some of the models in the TRENDY-N ensemble have the capability of
580 representing coupled C, N, and phosphorus (P) cycling (Goll et al., 2012; Nakhavali et al., 2022;
581 Sun et al., 2021; Wang et al., 2010, 2020b; Yang et al., 2014), P cycling was not active in the
582 model simulations in the GCP 2022. P limitation could be important for limiting terrestrial C
583 sequestration, especially in low-latitude forests (Elser et al., 2007; Terrer et al., 2019; Wieder et

584   al., 2015b). As more models incorporate coupled C-N-P cycling (Reed et al., 2015), observation-
585   based datasets of P will also be necessary for model evaluation.

586

587   **5 Conclusions**

588   Because the TRENDY-N ensemble overestimated both vegetation and soil C:N ratios, it
589   is possible that models could overestimate assimilated C per unit N and thus future terrestrial C
590   sequestration under CO_2 fertilisation. Alongside discrepancies in biological N fixation, this could
591   lead to biases in projections of the future terrestrial C sink by the TRENDY-N ensemble (not to
592   mention the other terrestrial biosphere models in the TRENDY ensemble that do not represent
593   coupled C-N cycling). While terrestrial biosphere models are capable of reproducing the current
594   terrestrial C sink, the results presented here suggest that underlying mechanisms of C-N cycling
595   interactions operate differently across models and may not be fully captured. These interactions
596   are critical for projections of the future terrestrial C sink as the C/N balance is expected to shift
597   in the future under interacting global change drivers.

Code availability

AMBER is available at https://gitlab.com/cseiler/AMBER.

Data availability

Biological N fixation, vegetation C:N ratio, and soil C:N ratio are available at
https://gitlab.com/siankg/amber-nitrogen.

Author contribution

SKG designed and conducted the study and prepared the initial manuscript. VA and CS provided
feedback on the initial manuscript and its subsequent revisions. The other co-authors conducted
TRENDY simulations and provided feedback on the manuscript.

Competing interests

The authors declare that they have no conflict of interest.

Acknowledgements

618 **Appendix A**
619
620 Table A1: IGBP land cover type, corresponding TRY plant trait database PFT, tissue C:N ratios
621 (from the TRY plant trait database (Kattge et al., 2020)), tissue fractions (Poorter et al., 2012),
622 and calculated total C:N ratio.

IGBP land cover type	TRY plant trait database PFT	Leaf C:N	Leaf fraction	Root C:N	Root fraction	Stem C:N	Stem fraction	Total C:N
0 bare	-							
1 Evergreen needleleaf forest	Tree evergreen needleleaf Temperate evergreen needleleaf Boreal evergreen needleleaf Gymnosperm evergreen needleleaf tree Temperate conifer Boreal conifer Evergreen gymnosperm	40.1	0.04	51.9	0.21	305.4	0.75	241.5
2 Evergreen broadleaf forest	Tree evergreen broadleaf Temperate evergreen broadleaf Tropical evergreen broadleaf Boreal evergreen broadleaf Angiosperm evergreen broadleaf tree Gymnosperm evergreen broadleaf tree Temperate evergreen Rainforest Evergreen angiosperm	26.8	0.02	26.4	0.16	139.3	0.82	119.0
3 Deciduous needleleaf forest	Tree deciduous needleleaf Boreal deciduous needleleaf Gymnosperm deciduous needleaf tree Deciduous gymnosperm							241.5[a]
4 Deciduous broadleaf forest	Tree deciduous broadleaf Temperate deciduous broadleaf Tropical deciduous broadleaf Boreal deciduous broadleaf Angiosperm deciduous broadleaf tree Gymnosperm deciduous broadleaf tree Temperate deciduous Deciduous angiosperm	21.5	0.03	39.6	0.21	102.1	0.76	86.6
5 Mixed forest								149.0[b]

6 Closed shrubland	Shrub evergreen broadleaf	34.5	0.09	24.9	0.47	216.7	0.49	121.0
7 Open shrubland	Evergreen shrub Deciduous shrub Shrub	34.5	0.09	24.9	0.47	216.7	0.49	121.0
8 Woody savannas	Angiosperm evergreen broadleaf shrub	34.5	0.09	24.9	0.36	216.7	0.57	134.5
9 Savannas	Angiosperm deciduous broadleaf shrub Gymnosperm evergreen broadleaf shrub Desert shrub Savanna evergreen Savanna deciduous	34.5	0.09	24.9	0.36	216.7	0.57	134.5
10 Grasslands	Grass C3 Grass C4 Temperate herbaceous Tropical herbaceous Herbaceous C3 Herbaceous C4 Angiosperm herbaceous C3 Angiosperm herbaceous C4	18.6	0.17	30.9	0.77	29.3	0.27	34.9
11 Permanent wetlands								34.9[c]
12 Croplands	Crop C3	11.7	0.17	30.9[c]	0.77	29.3[c]	0.27	28.9
13 Urban and built-up	-							
14 Cropland / natural vegetation mosaic								28.9[d]
15 Snow and ice	-							
16 Barren or sparsely vegetated	-							

623 [a] Value from evergreen needleleaf forest.
624 [b] Average of evergreen needleleaf forest, evergreen broadleaf forest, and deciduous broadleaf forest.
625 [c] Value from grasslands.
626 [d] Value from croplands.
627

628 Table A2: Kendall's tau from the Mann-Kendall test (p-value < 0.05) for each N pool and N flux
629 time series simulated by the TRENDY-N ensemble from 1850 to 2021. NS indicates that
630 Kendall's tau is not significant. NA indicates that the variable was not reported by the model.

	CABLE-POP	CLASSIC	CLM5.0	DLEM	ISAM	JSBACH	JULES-ES	LPJ-GUESS	LPX-Bern	OCNv2	ORCHIDEEv3
Vegetation N	0.58	NS	-0.97	-0.51	NS	0.83	NS	-0.25	-0.75	-0.67	-0.51
Litter N	0.88	0.15	0.65	-0.7	-0.87	0.92	0.86	-0.35	0.44	-0.69	NS
Soil N	1	-0.8	-0.47	-0.97	-0.91	0.99	-0.67	-0.68	1	1	-0.3
Biological N fixation	NS	0.95	0.84	-0.33	-0.11	0.89	0.79	0.62	0.92	0.45	NS
N uptake	0.89	0.64	0.81	0.78	NA	0.81	0.85	0.54	0.82	0.85	0.71
Net N mineralisation	0.91	0.33	0.73	0.87	NA	0.85	0.76	NS	0.86	0.82	0.31
N₂O emissions	NA	0.92	0.7	0.87	NA	0.95	NA	NA	0.7	0.42	0.69
N loss	NA	0.94	0.67	0.94	0.73	0.59	0.63	0.94	0.81	0.42	0.65

631

632   Table A3: Time-mean bias score (S_{bias}), spatial distribution score (S_{dist}), and overall score
633   ($S_{overall}$) of the TRENDY-N ensemble in simulating biological N fixation, vegetation C:N ratio,
634   and soil C:N ratio.

	Biological N fixation			Vegetation C:N ratio			Soil C:N ratio		
	S_{bias}	S_{dist}	$S_{overall}$	S_{bias}	S_{dist}	$S_{overall}$	S_{bias}	S_{dist}	$S_{overall}$
CABLE-POP	0.46	0.08	0.27	0.34	0.33	0.33	0.2	0.34	0.27
CLASSIC	0.46	0.4	0.43	0.45	0.59	0.52	0.43	0.22	0.33
CLM5.0	0.55	0.56	0.56	0.57	0.46	0.51	0.45	0.16	0.31
DLEM	0.46	0.29	0.38	0.47	0.75	0.61	0.48	0.01	0.24
ISAM	0.47	0.24	0.36	0.49	0.57	0.53	0.05	0.28	0.16
JSBACH	0.48	0.44	0.46	0.63	0.74	0.68	0.38	0.11	0.25
JULES-ES	0.47	0.43	0.45	0.4	0.49	0.44	0.51	0	0.25
LPJ-GUESS	0.51	0.45	0.48	0.45	0.52	0.48	0.49	0.01	0.25
LPX-Bern	NA	NA	NA	0.54	0.76	0.65	0.33	0.4	0.37
OCNv2	0.56	0.62	0.59	0.56	0.76	0.66	0.47	0.26	0.37
ORCHIDEEv3	0.6	0.63	0.61	0.27	0.41	0.34	0.48	0.31	0.39

635

636 Table A4: Overall scores of biological N fixation, vegetation C:N ratio, soil C:N ratio, and NBP
637 of TRENDY-N ensemble models with different representations of key N cycling processes (N
638 limitation of vegetation growth, biological N fixation, vegetation response to N limitation, and N
639 limitation of decomposition, see Table 1).

		BNF-DBFUSDA	CNVEG-TRY	CNSOIL-SoilGrids	NBP-CAMS	NBP-Carboscope	NBP-CT2019
N limitation of vegetation growth	V_{cmax} / flexible C:N stoichiometry	0.49	0.47	0.32	0.57	0.54	0.58
	NPP	0.41	0.58	0.26	0.56	0.52	0.58
	p-value	0.21	0.14	0.15	0.59	0.44	0.9
Biological N fixation	f(N limitation of vegetation growth)	0.44	0.34	0.33	0.57	0.54	0.57
	f(NPP) or f(ET)	0.44	0.53	0.23	0.57	0.54	0.6
	Time-invariant	0.53	0.56	0.33	0.57	0.55	0.59
	p-value	0.59	0.07	0.06	0.92	0.91	0.28
Vegetation response to N limitation	Dynamic	0.49	0.56	0.3	0.57	0.55	0.59
	Static	0.43	0.5	0.28	0.56	0.53	0.58
	p-value	0.44	0.41	0.71	0.48	0.3	0.67
N limitation of decomposition	f(soil N)	0.47	0.57	0.26	0.57	0.54	0.6
	N-invariant	0.45	0.46	0.32	0.56	0.52	0.56
	p-value	0.86	0.17	0.16	0.26	0.44	0.02

640

641 Table A5: Present-day global values of biological N fixation, vegetation C:N ratio, and soil C:N
642 ratio simulated by TRENDY-N ensemble models with different representations of key N cycling
643 processes (N limitation of vegetation growth, biological N fixation, vegetation response to N
644 limitation, and N limitation of decomposition, see Table 1).

		Biological N fixation	Vegetation C:N ratio	Soil C:N ratio
N limitation of vegetation growth	V_{cmax} / flexible C:N stoichiometry	106.78	161.8	12.75
	NPP	179.06	156.26	22.79
	p-value	0.51	0.85	0.39
Biological N fixation	f(N limitation of vegetation growth)	123.14	201.68	15.71
	f(NPP) or f(ET)	66.37	177.37	24.31
	Time-invariant	118.95	123.89	11.64
	p-value	0.27	0.15	0.68
Vegetation response to N limitation	Dynamic	99.25	143.32	11.22
	Static	173.29	172.58	22.4
	p-value	0.41	0.29	0.24
N limitation of decomposition	f(soil N)	88.21	153.36	20.04
	N-invariant	201.34	166.38	14.04
	p-value	0.3	0.66	0.53

645

646 Table A6: Kendall's tau from the Mann-Kendall test (p-value < 0.05) for biological N fixation,
647 vegetation C:N ratio, and soil C:N ratio simulated by TRENDY-N ensemble models with
648 different representations of key N cycling processes (N limitation of vegetation growth,
649 biological N fixation, vegetation response to N limitation, and N limitation of decomposition, see
650 Table 1).

		Biological N fixation	Vegetation C:N ratio	Soil C:N ratio
N limitation of vegetation growth	V_{cmax} / flexible C:N stoichiometry	0.48	-0.01	-0.04
	NPP	0.43	-0.74	0
	p-value	0.89	0.06	0.94
Biological N fixation	f(N limitation of vegetation growth)	0	-0.31	0.02
	f(NPP) or f(ET)	0.55	-0.6	0.14
	Time-invariant	0.74	0.39	-0.03
	p-value	0.15	0.15	0.97
Vegetation response to N limitation	Dynamic	0.5	-0.08	0.01
	Static	0.41	-0.56	-0.04
	p-value	0.77	0.3	0.93
N limitation of decomposition	f(soil N)	0.42	-0.42	0.31
	N-invariant	0.5	-0.25	-0.42
	p-value	0.8	0.7	0.14

651

Figure A1: Correlations between present-day global values (averaged over 1980–2021) of primary C and N pools and fluxes across TRENDY-N ensemble models: vegetation C (CVEG), litter C (CLITTER), soil C (CSOIL)), net biome productivity (NBP), gross primary productivity (GPP), autotrophic respiration (RA), heterotrophic respiration (RH), leaf area index (LAI), vegetation N (NVEG), litter N (NLITTER), soil N (NSOIL), biological N fixation (FBNF), N uptake (NUP), net N mineralisation (NETNMIN), N_2O emissions (N2O), N loss (NLOSS), vegetation C:N ratio (CNVEG), and soil C:N ratio (CNSOIL). Spearman's rank correlation coefficient is shown for statistically significant correlations (p-value < 0.05).

Figure A2: Correlations between Kendall's tau of primary C and N pools and fluxes across
TRENDY-N ensemble models: vegetation C (CVEG), litter C (CLITTER), soil C (CSOIL), net
biome productivity (NBP), gross primary productivity (GPP), autotrophic respiration (RA),
heterotrophic respiration (RH), leaf area index (LAI), vegetation N (NVEG), litter N
(NLITTER), soil N (NSOIL), biological N fixation (FBNF), N uptake (NUP), net N
mineralisation (NETNMIN), N$_2$O emissions (N2O), N loss (NLOSS), vegetation C:N ratio
(CNVEG), and soil C:N ratio (CNSOIL). Spearman's rank correlation coefficient is shown for
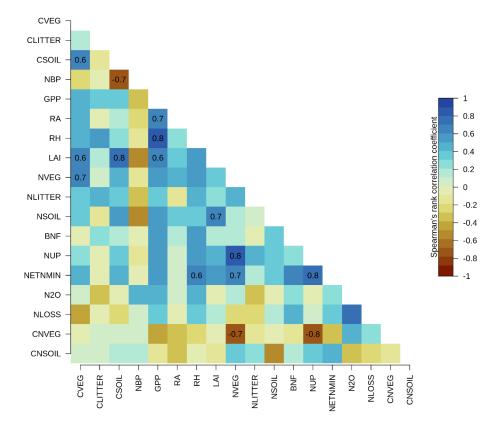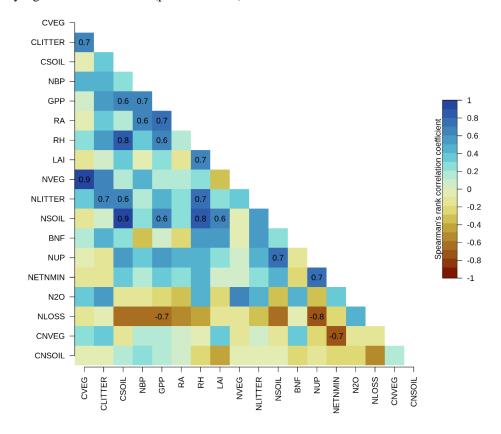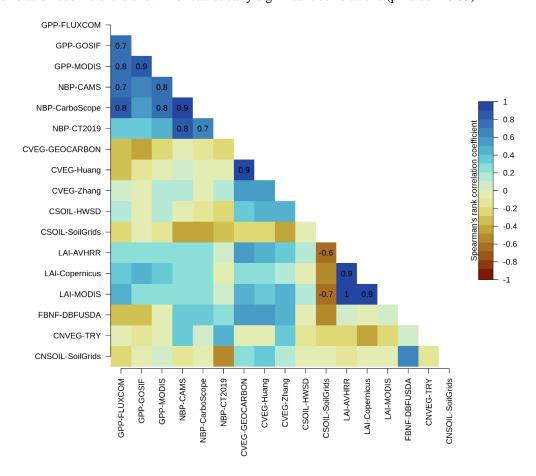statistically significant correlations (p-value < 0.05).

670 Figure A3: Correlations between overall scores of primary C and N pools and fluxes across
671 TRENDY-N ensemble models: gross primary productivity (GPP), net biome productivity (NBP),
672 vegetation C (CVEG), soil C (CSOIL), leaf area index (LAI), biological N fixation (FBNF),
673 vegetation C:N ratio (CNVEG), and soil C:N ratio (CNSOIL). Abbreviations of the observation-
674 based datasets are described in the Methods and in (Seiler et al., 2022). Spearman's rank
675 correlation coefficient is shown for statistically significant correlations (p-value < 0.05).

676

677   Figure A4: Time series of a. vegetation N, b. litter N, c. soil N, d. biological N fixation, e. N
678   uptake, f. net N mineralisation, g. N$_2$O emissions, and h. N loss simulated by the TRENDY-N
679   ensemble from 1850 to 2021.
680

681

682   Figure A5: Latitudinal distributions and global means of ab. biological N fixation, cd. vegetation
683   C:N ratio, and ef. soil C:N ratio simulated by the TRENDY-N ensemble (averaged across models
684   over 1980–2021) in comparison to observation-based datasets from (Davies-Barnard and
685   Friedlingstein, 2020) for biological N fixation, the TRY plant trait database for vegetation C:N
686   ratio, and SoilGrids for soil C:N ratio. Boxplots show the median, interquartile range (box), and
687   80% percentiles (whiskers) of the global mean.

688

References

689 **References**

690 Agustí-Panareda, A., Diamantakis, M., Massart, S., Chevallier, F., Muñoz-Sabater, J., Barré, J., Curcoll,
691 R., Engelen, R., Langerock, B., Law, R. M., Loh, Z., Morguí, J. A., Parrington, M., Peuch, V.-H.,
692 Ramonet, M., Roehl, C., Vermeulen, A. T., Warneke, T., and Wunch, D.: Modelling CO_2 weather – why
693 horizontal resolution matters, Atmospheric Chem. Phys., 19, 7347–7376, https://doi.org/10.5194/acp-19-
694 7347-2019, 2019.

695 Avitabile, V., Herold, M., Heuvelink, G. B. M., Lewis, S. L., Phillips, O. L., Asner, G. P., Armston, J.,
696 Ashton, P. S., Banin, L., Bayol, N., Berry, N. J., Boeckx, P., de Jong, B. H. J., DeVries, B., Girardin, C.
697 A. J., Kearsley, E., Lindsell, J. A., Lopez-Gonzalez, G., Lucas, R., Malhi, Y., Morel, A., Mitchard, E. T.
698 A., Nagy, L., Qie, L., Quinones, M. J., Ryan, C. M., Ferry, S. J. W., Sunderland, T., Laurin, G. V., Gatti,
699 R. C., Valentini, R., Verbeeck, H., Wijaya, A., and Willcock, S.: An integrated pan-tropical biomass map
700 using multiple reference datasets, Glob. Change Biol., 22, 1406–1420, https://doi.org/10.1111/gcb.13139,
701 2016.

702 Barron, A. R., Purves, D. W., and Hedin, L. O.: Facultative nitrogen fixation by canopy legumes in a
703 lowland tropical forest, Oecologia, 165, 511–520, https://doi.org/10.1007/s00442-010-1838-3, 2011.

704 Barton, L., Wolf, B., Rowlings, D., Scheer, C., Kiese, R., Grace, P., Stefanova, K., and Butterbach-Bahl,
705 K.: Sampling frequency affects estimates of annual nitrous oxide fluxes, Sci. Rep., 5, 1–9,
706 https://doi.org/10.1038/srep15912, 2015.

707 Batjes, N. H., Ribeiro, E., and van Oostrum, A.: Standardised soil profile data to support global mapping
708 and modelling (WoSIS snapshot 2019), Earth Syst. Sci. Data, 12, 299–320, https://doi.org/10.5194/essd-
709 12-299-2020, 2020.

710 Batterman, S. A., Hedin, L. O., Breugel, M. van, Ransijn, J., Craven, D. J., and Hall, J. S.: Key role of
711 symbiotic dinitrogen fixation in tropical forest secondary succession, Nature, 502, 224–227,
712 https://doi.org/10.1038/nature12525, 2013.

713 Chini, L., Hurtt, G., Sahajpal, R., Frolking, S., Goldewijk, K. K., Sitch, S., Ganzenmüller, R., Ma, L., Ott,
714 L., Pongratz, J., and Poulter, B.: Land-use harmonization datasets for annual global carbon budgets, Earth
715 Syst. Sci. Data, 13, 4175–4189, https://doi.org/10.5194/essd-13-4175-2021, 2021.

716 Claverie, M., Matthews, J. L., Vermote, E. F., and Justice, C. O.: A 30+ Year AVHRR LAI and FAPAR
717 Climate Data Record: Algorithm Description and Validation, Remote Sens., 8,
718 https://doi.org/10.3390/rs8030263, 2016.

719 Cleveland, C. C., Townsend, A. R., Schimel, D. S., Fisher, H., Hedin, L. O., Perakis, S., Latty, E. F.,
720 Fischer, C. V., Elseroad, A., and Wasson, M. F.: Global patterns of terrestrial biological nitrogen (N_2)
721 fixation in natural ecosystems, Glob. Biochem. Cycles, 13, 623–645,
722 https://doi.org/10.1029/1999GB900014, 1999.

723 Collier, N., Hoffman, F. M., Lawrence, D. M., Keppel-Aleks, G., Koven, C. D., Riley, W. J., Mu, M., and
724 Randerson, J. T.: The International Land Model Benchmarking (ILAMB) System: Design, Theory, and
725 Implementation, J. Adv. Model. Earth Syst., 10, 2731–2754, https://doi.org/10.1029/2018MS001354,
726 2018.

727 Cotrufo, M. F., Wallenstein, M. D., Boot, C. M., Denef, K., and Paul, E.: The Microbial Efficiency-
728 Matrix Stabilization (MEMS) framework integrates plant litter decomposition with soil organic matter

729   stabilization: Do labile plant inputs form stable soil organic matter?, Glob. Change Biol., 19, 988–995,
730   https://doi.org/10.1111/gcb.12113, 2013.

731   Davies-Barnard, T. and Friedlingstein, P.: The Global Distribution of Biological Nitrogen Fixation in
732   Terrestrial Natural Ecosystems, Glob. Biogeochem. Cycles, 34, 1–17,
733   https://doi.org/10.1029/2019GB006387, 2020.

734   Davies-Barnard, T., Meyerholt, J., Zaehle, S., Friedlingstein, P., Brovkin, V., Fan, Y., Fisher, R. A.,
735   Jones, C. D., Lee, H., Peano, D., Smith, B., Wärlind, D., and Wiltshire, A. J.: Nitrogen cycling in CMIP6
736   land surface models: Progress and limitations, Biogeosciences, 17, 5129–5148,
737   https://doi.org/10.5194/bg-17-5129-2020, 2020.

738   Dlugokencky, E. and Tans, P.: Trends in atmospheric carbon dioxide, National Oceanic and Atmospheric
739   Administration, Global Monitoring Laboratory (NOAA/GML), 2022.

740   Du, E., Terrer, C., Pellegrini, A. F. A., Ahlstrom, A., Lissa, C. J. van, Zhao, X., Xia, N., Wu, X., and
741   Jackson, R. B.: Global patterns of terrestrial nitrogen and phosphorus limitation, Nat. Geosci., 13, 221–
742   226, https://doi.org/10.1038/s41561-019-0530-4, 2020.

743   Elser, J. J., Bracken, M. E. S., Cleland, E. E., Gruner, D. S., Harpole, W. S., Hillebrand, H., Ngai, J. T.,
744   Seabloom, E. W., Shurin, J. B., and Smith, J. E.: Global analysis of nitrogen and phosphorus limitation of
745   primary producers in freshwater, marine and terrestrial ecosystems, Ecol. Lett., 10, 1135–1142,
746   https://doi.org/10.1111/j.1461-0248.2007.01113.x, 2007.

747   Elser, J. J., Fagan, W. F., Kerkhoff, A. J., Swenson, N. G., and Enquist, B. J.: Biological stoichiometry of
748   plant production: Metabolism, scaling and ecological response to global change, New Phytol., 186, 593–
749   608, https://doi.org/10.1111/j.1469-8137.2010.03214.x, 2010.

750   Fernández-Martínez, M., Vicca, S., Janssens, I. A., Sardans, J., Luyssaert, S., Campioli, M., Chapin, F. S.,
751   Ciais, P., Malhi, Y., Obersteiner, M., Papale, D., Piao, S. L., Reichstein, M., Rodà, F., and Peñuelas, J.:
752   Nutrient availability as the key regulator of global forest carbon balance, Nat. Clim. Change, 4, 471–476,
753   https://doi.org/10.1038/nclimate2177, 2014.

754   Fisher, R. A. and Koven, C. D.: Perspectives on the Future of Land Surface Models and the Challenges of
755   Representing Complex Terrestrial Systems, J. Adv. Model. Earth Syst., 12,
756   https://doi.org/10.1029/2018MS001453, 2020.

757   Fowler, D., Coyle, M., Skiba, U., Sutton, M. A., Cape, J. N., Reis, S., Sheppard, L. J., Jenkins, A.,
758   Grizzetti, B., Galloway, J. N., Vitousek, P., Leach, A., Bouwman, A. F., Butterbach-Bahl, K., Dentener,
759   F., Stevenson, D., Amann, M., and Voss, M.: The global nitrogen cycle in the twenty-first century, Philos.
760   Trans. R. Soc. B Biol. Sci., 368, 20130164, https://doi.org/10.1098/rstb.2013.0164, 2013.

761   Friedl, M. A., Sulla-Menashe, D., Tan, B., Schneider, A., Ramankutty, N., Sibley, A., and Huang, X.:
762   MODIS Collection 5 global land cover: Algorithm refinements and characterization of new datasets,
763   Remote Sens. Environ., 114, 168–182, https://doi.org/10.1016/j.rse.2009.08.016, 2010.

764   Friedlingstein, P., O'Sullivan, M., Jones, M. W., Andrew, R. M., Gregor, L., Hauck, J., Le Quéré, C.,
765   Luijkx, I. T., Olsen, A., Peters, G. P., Peters, W., Pongratz, J., Schwingshackl, C., Sitch, S., Canadell, J.
766   G., Ciais, P., Jackson, R. B., Alin, S. R., Alkama, R., Arneth, A., Arora, V. K., Bates, N. R., Becker, M.,
767   Bellouin, N., Bittig, H. C., Bopp, L., Chevallier, F., Chini, L. P., Cronin, M., Evans, W., Falk, S., Feely,
768   R. A., Gasser, T., Gehlen, M., Gkritzalis, T., Gloege, L., Grassi, G., Gruber, N., Gürses, Ö., Harris, I.,

769   Hefner, M., Houghton, R. A., Hurtt, G. C., Iida, Y., Ilyina, T., Jain, A. K., Jersild, A., Kadono, K., Kato,
770   E., Kennedy, D., Klein Goldewijk, K., Knauer, J., Korsbakken, J. I., Landschützer, P., Lefèvre, N.,
771   Lindsay, K., Liu, J., Liu, Z., Marland, G., Mayot, N., McGrath, M. J., Metzl, N., Monacci, N. M., Munro,
772   D. R., Nakaoka, S.-I., Niwa, Y., O'Brien, K., Ono, T., Palmer, P. I., Pan, N., Pierrot, D., Pocock, K.,
773   Poulter, B., Resplandy, L., Robertson, E., Rödenbeck, C., Rodriguez, C., Rosan, T. M., Schwinger, J.,
774   Séférian, R., Shutler, J. D., Skjelvan, I., Steinhoff, T., Sun, Q., Sutton, A. J., Sweeney, C., Takao, S.,
775   Tanhua, T., Tans, P. P., Tian, X., Tian, H., Tilbrook, B., Tsujino, H., Tubiello, F., van der Werf, G. R.,
776   Walker, A. P., Wanninkhof, R., Whitehead, C., Willstrand Wranne, A., et al.: Global Carbon Budget
777   2022, Earth Syst. Sci. Data, 14, 4811–4900, https://doi.org/10.5194/essd-14-4811-2022, 2022.

778   Goll, D. S., Brovkin, V., Parida, B. R., Reick, C. H., Kattge, J., Reich, P. B., Bodegom, P. M. V., and
779   Niinemets, Ü.: Nutrient limitation reduces land carbon uptake in simulations with a model of combined
780   carbon, nitrogen and phosphorus cycling, Biogeosciences, 9, 3547–3569, https://doi.org/10.5194/bg-9-
781   3547-2012, 2012.

782   Han, W., Tang, L., Chen, Y., and Fang, J.: Relationship between the relative limitation and resorption
783   efficiency of nitrogen vs phosphorus in woody plants, PLoS ONE, 8, e83366,
784   https://doi.org/10.1371/journal.pone.0083366, 2013.

785   Harris, I., Osborn, T. J., Jones, P., and Lister, D.: Version 4 of the CRU TS monthly high-resolution
786   gridded multivariate climate dataset, Sci. Data, 7, 1–18, https://doi.org/10.1038/s41597-020-0453-3,
787   2020.

788   Haverd, V., Smith, B., Nieradzik, L., Briggs, P. R., Woodgate, W., Trudinger, C. M., Canadell, J. G., and
789   Cuntz, M.: A new version of the CABLE land surface model (Subversion revision r4601) incorporating
790   land use and land cover change, woody vegetation demography, and a novel optimisation-based approach
791   to plant coordination of photosynthesis, Geosci. Model Dev., 11, 2995–3026,
792   https://doi.org/10.5194/gmd-11-2995-2018, 2018.

793   Hedin, L. O., Brookshire, E. N. J., Menge, D. N. L., and Barron, A. R.: The Nitrogen Paradox in Tropical
794   Forest Ecosystems, Annu. Rev. Ecol. Evol. Syst., 40, 613–635,
795   https://doi.org/10.1146/annurev.ecolsys.37.091305.110246, 2009.

796   Hegglin, M., Kinnison, D., and Lamarque, J.-F.: CCMI nitrogen surface fluxes in support of CMIP6 -
797   version 2.0, https://doi.org/10.22033/ESGF/input4MIPs.1125, 2016.

798   Hengl, T., Jesus, J. M. D., Heuvelink, G. B. M., Gonzalez, M. R., Kilibarda, M., Blagotić, A., Shangguan,
799   W., Wright, M. N., Geng, X., Bauer-Marschallinger, B., Guevara, M. A., Vargas, R., MacMillan, R. A.,
800   Batjes, N. H., Leenaars, J. G. B., Ribeiro, E., Wheeler, I., Mantel, S., and Kempen, B.: SoilGrids250m:
801   Global gridded soil information based on machine learning, PLoS ONE, 12, e0169748,
802   https://doi.org/10.1371/journal.pone.0169748, 2017.

803   Herridge, D. F., Peoples, M. B., and Boddey, R. M.: Global inputs of biological nitrogen fixation in
804   agricultural systems, Plant Soil, 311, 1–18, https://doi.org/10.1007/s11104-008-9668-3, 2008.

805   Hipel, K. W. and McLeod, A. I.: Time series modelling of water resources and environmental systems,
806   Elsevier, 1994.

807   Houlton, B. Z., Morford, S. L., and Dahlgren, R. A.: Convergent evidence for widespread rock nitrogen
808   sources in Earth's surface environment, Science, 360, 58–62, https://doi.org/10.1126/science.aan4399,
809   2018.

810 Huang, Y., Ciais, P., Santoro, M., Makowski, D., Chave, J., Schepaschenko, D., Abramoff, R. Z., Goll, D.
811 S., Yang, H., Chen, Y., Wei, W., and Piao, S.: A global map of root biomass across the world's forests,
812 Earth Syst. Sci. Data, 13, 4263–4274, https://doi.org/10.5194/essd-13-4263-2021, 2021.

813 Hungate, B. A., Dukes, J. S., Shaw, M. R., Luo, Y., and Field, C. B.: Nitrogen and Climate Change,
814 Science, 302, 1512–1513, 2003.

815 Huntzinger, D. N., Michalak, A. M., Schwalm, C., Ciais, P., King, A. W., Fang, Y., Schaefer, K., Wei,
816 Y., Cook, R. B., Fisher, J. B., Hayes, D., Huang, M., Ito, A., Jain, A. K., Lei, H., Lu, C., Maignan, F.,
817 Mao, J., Parazoo, N., Peng, S., Poulter, B., Ricciuto, D., Shi, X., Tian, H., Wang, W., Zeng, N., and Zhao,
818 F.: Uncertainty in the response of terrestrial carbon sink to environmental drivers undermines carbon-
819 climate feedback predictions, Sci. Rep., 7, 1–8, https://doi.org/10.1038/s41598-017-03818-2, 2017.

820 Hurtt, G. C., Chini, L., Sahajpal, R., Frolking, S., Bodirsky, B. L., Calvin, K., Doelman, J. C., Fisk, J.,
821 Fujimori, S., Klein Goldewijk, K., Hasegawa, T., Havlik, P., Heinimann, A., Humpenöder, F., Jungclaus,
822 J., Kaplan, J. O., Kennedy, J., Krisztin, T., Lawrence, D., Lawrence, P., Ma, L., Mertz, O., Pongratz, J.,
823 Popp, A., Poulter, B., Riahi, K., Shevliakova, E., Stehfest, E., Thornton, P., Tubiello, F. N., van Vuuren,
824 D. P., and Zhang, X.: Harmonization of global land use change and management for the period 850–2100
825 (LUH2) for CMIP6, Geosci. Model Dev., 13, 5425–5464, https://doi.org/10.5194/gmd-13-5425-2020,
826 2020.

827 Jacobson, A. R., Schuldt, K. N., Miller, J. B., Oda, T., Tans, P., Andrews, A., Mund, J., Ott, L., Collatz,
828 G. J., and Aalto, T.: CarbonTracker CT2019, NOAA Earth Syst. Res. Lab. Glob. Monit. Div., 10, 2020.

829 Joos, F., Spahni, R., Stocker, B. D., Lienert, S., Müller, J., Fischer, H., Schmitt, J., Prentice, I. C., Otto-
830 Bliesner, B., and Liu, Z.: N$_2$O changes from the Last Glacial Maximum to the preindustrial – Part 2:
831 terrestrial N$_2$O emissions and carbon–nitrogen cycle interactions, Biogeosciences, 17, 3511–3543,
832 https://doi.org/10.5194/bg-17-3511-2020, 2020.

833 Jung, M., Schwalm, C., Migliavacca, M., Walther, S., Camps-Valls, G., Koirala, S., Anthoni, P., Besnard,
834 S., Bodesheim, P., Carvalhais, N., Chevallier, F., Gans, F., Goll, D. S., Haverd, V., Köhler, P., Ichii, K.,
835 Jain, A. K., Liu, J., Lombardozzi, D., Nabel, J. E. M. S., Nelson, J. A., O'Sullivan, M., Pallandt, M.,
836 Papale, D., Peters, W., Pongratz, J., Rödenbeck, C., Sitch, S., Tramontana, G., Walker, A., Weber, U., and
837 Reichstein, M.: Scaling carbon fluxes from eddy covariance sites to globe: synthesis and evaluation of the
838 FLUXCOM approach, Biogeosciences, 17, 1343–1365, https://doi.org/10.5194/bg-17-1343-2020, 2020.

839 Kattge, J., Bönisch, G., Díaz, S., Lavorel, S., Prentice, I. C., Leadley, P., Tautenhahn, S., Werner, G. D.
840 A., Aakala, T., Abedi, M., Acosta, A. T. R., Adamidis, G. C., Adamson, K., Aiba, M., Albert, C. H.,
841 Alcántara, J. M., C, C. A., Aleixo, I., Ali, H., Amiaud, B., Ammer, C., Amoroso, M. M., Anand, M.,
842 Anderson, C., Anten, N., Antos, J., Apgaua, D. M. G., Ashman, T. L., Asmara, D. H., Asner, G. P.,
843 Aspinwall, M., Atkin, O., Aubin, I., Baastrup-Spohr, L., Bahalkeh, K., Bahn, M., Baker, T., Baker, W. J.,
844 Bakker, J. P., Baldocchi, D., Baltzer, J., Banerjee, A., Baranger, A., Barlow, J., Barneche, D. R., Baruch,
845 Z., Bastianelli, D., Battles, J., Bauerle, W., Bauters, M., Bazzato, E., Beckmann, M., Beeckman, H.,
846 Beierkuhnlein, C., Bekker, R., Belfry, G., Belluau, M., Beloiu, M., Benavides, R., Benomar, L., Berdugo-
847 Lattke, M. L., Berenguer, E., Bergamin, R., Bergmann, J., Carlucci, M. B., Berner, L., Bernhardt-
848 Römermann, M., Bigler, C., Bjorkman, A. D., Blackman, C., Blanco, C., Blonder, B., Blumenthal, D.,
849 Bocanegra-González, K. T., Boeckx, P., Bohlman, S., Böhning-Gaese, K., Boisvert-Marsh, L., Bond, W.,
850 Bond-Lamberty, B., Boom, A., Boonman, C. C. F., Bordin, K., Boughton, E. H., Boukili, V., Bowman,
851 D. M. J. S., Bravo, S., Brendel, M. R., Broadley, M. R., Brown, K. A., Bruelheide, H., Brumnich, F.,
852 Bruun, H. H., Bruy, D., Buchanan, S. W., Bucher, S. F., Buchmann, N., Buitenwerf, R., Bunker, D. E., et

853 al.: TRY plant trait database – enhanced coverage and open access, Glob. Change Biol., 26, 119–188,
854 https://doi.org/10.1111/gcb.14904, 2020.

855 Klein Goldewijk, K., Beusen, A., Doelman, J., and Stehfest, E.: Anthropogenic land use estimates for the
856 Holocene – HYDE 3.2, Earth Syst. Sci. Data, 9, 927–953, https://doi.org/10.5194/essd-9-927-2017,
857 2017a.

858 Klein Goldewijk, K., Dekker, S. C., and Zanden, J. L. van: Per-capita estimations of long-term historical
859 land use and the consequences for global change research, J. Land Use Sci., 12, 313–337,
860 https://doi.org/10.1080/1747423X.2017.1354938, 2017b.

861 Knyazikhin, Y., Schull, M. A., Stenberg, P., Mõttus, M., Rautiainen, M., Yang, Y., Marshak, A., Latorre
862 Carmona, P., Kaufmann, R. K., Lewis, P., Disney, M. I., Vanderbilt, V., Davis, A. B., Baret, F.,
863 Jacquemoud, S., Lyapustin, A., and Myneni, R. B.: Hyperspectral remote sensing of foliar nitrogen
864 content, Proc. Natl. Acad. Sci., 110, E185–E192, https://doi.org/10.1073/pnas.1210196109, 2013.

865 Kobe, R. K., Lepczyk, C. A., and Iyer, M.: Resorption efficiency decreases with increasing green leaf
866 nutrients in a global data set, Ecology, 86, 2780–2792, 2005.

867 Kou-Giesbrecht, S. and Arora, V. K.: Representing the Dynamic Response of Vegetation to Nitrogen
868 Limitation via Biological Nitrogen Fixation in the CLASSIC Land Model, Glob. Biogeochem. Cycles,
869 36, e2022GB007341, https://doi.org/10.1029/2022GB007341, 2022.

870 Lawrence, D. M., Fisher, R. A., Koven, C. D., Oleson, K. W., Swenson, S. C., Bonan, G., Collier, N.,
871 Ghimire, B., Kampenhout, L. van, Kennedy, D., Kluzek, E., Lawrence, P. J., Li, F., Li, H., Lombardozzi,
872 D., Riley, W. J., Sacks, W. J., Shi, M., Vertenstein, M., Wieder, W. R., Xu, C., Ali, A. A., Badger, A. M.,
873 Bisht, G., Broeke, M. van den, Brunke, M. A., Burns, S. P., Buzan, J., Clark, M., Craig, A., Dahlin, K.,
874 Drewniak, B., Fisher, J. B., Flanner, M., Fox, A. M., Gentine, P., Hoffman, F., Keppel-Aleks, G., Knox,
875 R., Kumar, S., Lenaerts, J., Leung, L. R., Lipscomb, W. H., Lu, Y., Pandey, A., Pelletier, J. D., Perket, J.,
876 Randerson, J. T., Ricciuto, D. M., Sanderson, B. M., Slater, A., Subin, Z. M., Tang, J., Thomas, R. Q.,
877 Martin, M. V., and Zeng, X.: The Community Land Model Version 5: Description of New Features,
878 Benchmarking, and Impact of Forcing Uncertainty, J. Adv. Model. Earth Syst., 11, 4245–4287,
879 https://doi.org/10.1029/2018MS001583, 2019.

880 LeBauer, D. S. and Treseder, K. K.: Nitrogen Limitation of Net Primary Productivity in Terrestrial
881 Ecosystems is Globally Distributed, Ecology, 89, 371–379, https://doi.org/10.1016/j.agee.2013.04.020,
882 2008.

883 Li, X. and Xiao, J.: Mapping Photosynthesis Solely from Solar-Induced Chlorophyll Fluorescence: A
884 Global, Fine-Resolution Dataset of Gross Primary Production Derived from OCO-2, Remote Sens., 11,
885 https://doi.org/10.3390/rs11212563, 2019.

886 Lienert, S. and Joos, F.: A Bayesian ensemble data assimilation to constrain model parameters and land-
887 use carbon emissions, Biogeosciences, 15, 2909–2930, https://doi.org/10.5194/bg-15-2909-2018, 2018.

888 Liu, Y., Wang, C., He, N., Wen, X., Gao, Y., Li, S., Niu, S., Butterbach-Bahl, K., Luo, Y., and Yu, G.: A
889 global synthesis of the rate and temperature sensitivity of soil nitrogen mineralization: latitudinal patterns
890 and mechanisms, Glob. Change Biol., 23, 455–464, https://doi.org/10.1111/gcb.13372, 2017.

891 Medlyn, B. E., Zaehle, S., Kauwe, M. G. D., Walker, A. P., Dietze, M. C., Hanson, P. J., Hickler, T., Jain,
892 A. K., Luo, Y., Parton, W., Prentice, I. C., Thornton, P. E., Wang, S., Wang, Y. P., Weng, E., Iversen, C.

893 M., Mccarthy, H. R., Warren, J. M., Oren, R., and Norby, R. J.: Using ecosystem experiments to improve
894 vegetation models, Nat. Clim. Change, 5, 528–534, https://doi.org/10.1038/nclimate2621, 2015.

895 Melton, J. R., Arora, V. K., Wisernig-Cojoc, E., Seiler, C., Fortier, M., Chan, E., and Teckentrup, L.:
896 CLASSIC v1.0: The open-source community successor to the Canadian Land Surface Scheme (CLASS)
897 and the Canadian Terrestrial Ecosystem Model (CTEM)-Part 1: Model framework and site-level
898 performance, Geosci. Model Dev., 13, 2825–2850, https://doi.org/10.5194/gmd-13-2825-2020, 2020.

899 Menge, D. N. L., Wolf, A. A., and Funk, J. L.: Diversity of nitrogen fixation strategies in Mediterranean
900 legumes, Nat. Plants, 1, 1–5, https://doi.org/10.1038/nplants.2015.64, 2015.

901 Meyerholt, J., Zaehle, S., and Smith, M. J.: Variability of projected terrestrial biosphere responses to
902 elevated levels of atmospheric CO2 due to uncertainty in biological nitrogen fixation, Biogeosciences, 13,
903 1491–1518, https://doi.org/10.5194/bg-13-1491-2016, 2016.

904 Meyerholt, J., Sickel, K., and Zaehle, S.: Ensemble projections elucidate effects of uncertainty in
905 terrestrial nitrogen limitation on future carbon uptake, Glob. Change Biol., 26, 3978–3996,
906 https://doi.org/10.1111/gcb.15114, 2020.

907 Myneni, R. B., Hoffman, S., Knyazikhin, Y., Privette, J. L., Glassy, J., Tian, Y., Wang, Y., Song, X.,
908 Zhang, Y., Smith, G. R., Lotsch, A., Friedl, M., Morisette, J. T., Votava, P., Nemani, R. R., and Running,
909 S. W.: Global products of vegetation leaf area and fraction absorbed PAR from year one of MODIS data,
910 Moderate Resolut. Imaging Spectroradiometer MODIS New Gener. Land Surf. Monit., 83, 214–231,
911 https://doi.org/10.1016/S0034-4257(02)00074-3, 2002.

912 Nakhavali, M. A., Mercado, L. M., Hartley, I. P., Sitch, S., Cunha, F. V., di Ponzio, R., Lugli, L. F.,
913 Quesada, C. A., Andersen, K. M., Chadburn, S. E., Wiltshire, A. J., Clark, D. B., Ribeiro, G., Siebert, L.,
914 Moraes, A. C. M., Schmeisk Rosa, J., Assis, R., and Camargo, J. L.: Representation of the phosphorus
915 cycle in the Joint UK Land Environment Simulator (vn5.5_JULES-CNP), Geosci. Model Dev., 15, 5241–
916 5269, https://doi.org/10.5194/gmd-15-5241-2022, 2022.

917 O'Sullivan, M., Spracklen, D. V., Batterman, S. A., Arnold, S. R., Gloor, M., and Buermann, W.: Have
918 Synergies Between Nitrogen Deposition and Atmospheric CO_2 Driven the Recent Enhancement of the
919 Terrestrial Carbon Sink?, Glob. Biogeochem. Cycles, 33, 163–180,
920 https://doi.org/10.1029/2018GB005922, 2019.

921 Peng, J., Wang, Y. P., Houlton, B. Z., Dan, L., Pak, B., and Tang, X.: Global Carbon Sequestration Is
922 Highly Sensitive to Model-Based Formulations of Nitrogen Fixation, Glob. Biogeochem. Cycles, 34,
923 e2019GB006296, https://doi.org/10.1029/2019GB006296, 2020.

924 Phillips, R. P., Brzostek, E., and Midgley, M. G.: The mycorrhizal-associated nutrient economy: A new
925 framework for predicting carbon-nutrient couplings in temperate forests, New Phytol., 199, 41–51,
926 https://doi.org/10.1111/nph.12221, 2013.

927 Poggio, L., de Sousa, L. M., Batjes, N. H., Heuvelink, G. B. M., Kempen, B., Ribeiro, E., and Rossiter,
928 D.: SoilGrids 2.0: producing soil information for the globe with quantified spatial uncertainty, SOIL, 7,
929 217–240, https://doi.org/10.5194/soil-7-217-2021, 2021.

930 Poorter, H., Niklas, K. J., Reich, P. B., Oleksyn, J., Poot, P., and Mommer, L.: Biomass allocation to
931 leaves, stems and roots: Meta-analyses of interspecific variation and environmental control, New Phytol.,
932 193, 30–50, https://doi.org/10.1111/j.1469-8137.2011.03952.x, 2012.

933   Reed, S. C., Cleveland, C. C., and Townsend, A. R.: Functional Ecology of Free-Living Nitrogen
934   Fixation: A Contemporary Perspective, Annu. Rev. Ecol. Evol. Syst., 42, 489–512,
935   https://doi.org/10.1146/annurev-ecolsys-102710-145034, 2011.

936   Reed, S. C., Yang, X., and Thornton, P. E.: Incorporating phosphorus cycling into global modeling
937   efforts: A worthwhile, tractable endeavor, New Phytol., 208, 324–329, https://doi.org/10.1111/nph.13521,
938   2015.

939   Reick, C. H., Gayler, V., Goll, D., Hagemann, S., Heidkamp, M., Nabel, J. E., Raddatz, T., Roeckner, E.,
940   Schnur, R., and Wilkenskjeld, S.: JSBACH 3-The land component of the MPI Earth System Model:
941   documentation of version 3.2, 2021.

942   Rödenbeck, C., Zaehle, S., Keeling, R., and Heimann, M.: How does the terrestrial carbon exchange
943   respond to inter-annual climatic variations? A quantification based on atmospheric CO_2 data,
944   Biogeosciences, 15, 2481–2498, https://doi.org/10.5194/bg-15-2481-2018, 2018.

945   Santoro, M., Beaudoin, A., Beer, C., Cartus, O., Fransson, J. E. S., Hall, R. J., Pathe, C., Schmullius, C.,
946   Schepaschenko, D., Shvidenko, A., Thurner, M., and Wegmüller, U.: Forest growing stock volume of the
947   northern hemisphere: Spatially explicit estimates for 2010 derived from Envisat ASAR, Remote Sens.
948   Environ., 168, 316–334, https://doi.org/10.1016/j.rse.2015.07.005, 2015.

949   Seiler, C., Melton, J., Arora, V., and Wang, L.: CLASSIC v1.0: the open-source community successor to
950   the Canadian Land Surface Scheme (CLASS) and the Canadian Terrestrial Ecosystem Model (CTEM) –
951   Part 2: Global Benchmarking, Geosci. Model Dev., 14, 2371–2417, https://doi.org/10.5194/gmd-2020-
952   294, 2021.

953   Seiler, C., Melton, J. R., Arora, V. K., Sitch, S., Friedlingstein, P., Anthoni, P., Goll, D., Jain, A. K.,
954   Joetzjer, E., Lienert, S., Lombardozzi, D., Luyssaert, S., Nabel, J. E. M. S., Tian, H., Vuichard, N.,
955   Walker, A. P., Yuan, W., and Zaehle, S.: Are Terrestrial Biosphere Models Fit for Simulating the Global
956   Land Carbon Sink?, J. Adv. Model. Earth Syst., 14, e2021MS002946,
957   https://doi.org/10.1029/2021MS002946, 2022.

958   Shu, S., Jain, A. K., Koven, C. D., and Mishra, U.: Estimation of Permafrost SOC Stock and Turnover
959   Time Using a Land Surface Model With Vertical Heterogeneity of Permafrost Soils, Glob. Biogeochem.
960   Cycles, 34, e2020GB006585, https://doi.org/10.1029/2020GB006585, 2020.

961   Smith, B., Wårlind, D., Arneth, A., Hickler, T., Leadley, P., Siltberg, J., and Zaehle, S.: Implications of
962   incorporating N cycling and N limitations on primary production in an individual-based dynamic
963   vegetation model, Biogeosciences, 11, 2027–2054, https://doi.org/10.5194/bg-11-2027-2014, 2014.

964   Soper, F. M., Taylor, B. N., Winbourne, J. B., Wong, M. Y., Dynarski, K. A., Reis, C. R. G., Peoples, M.
965   B., Cleveland, C. C., Reed, S. C., Menge, D. N. L., and Perakis, S. S.: A roadmap for sampling and
966   scaling biological nitrogen fixation in terrestrial ecosystems, Methods Ecol. Evol., 2021, 1–16,
967   https://doi.org/10.1111/2041-210X.13586, 2021.

968   Stocker, B. D., Prentice, I. C., Cornell, S. E., Davies-Barnard, T., Finzi, A. C., Franklin, O., Janssens, I.,
969   Larmola, T., Manzoni, S., Näsholm, T., Raven, J. A., Rebel, K. T., Reed, S., Vicca, S., Wiltshire, A., and
970   Zaehle, S.: Terrestrial nitrogen cycling in Earth system models revisited, New Phytol., 210, 1165–1168,
971   https://doi.org/10.1111/nph.13997, 2016.

972 Sullivan, B. W., Smith, W. K., Alan, R., Nasto, M. K., Reed, S. C., and Chazdon, R. L.: Spatially robust
973 estimates of biological nitrogen (N) fixation imply substantial human alteration of the tropical N cycle,
974 Proc. Natl. Acad. Sci., 111, 8101–8106, https://doi.org/10.1073/pnas.1511978112, 2014.

975 Sun, Y., Goll, D. S., Chang, J., Ciais, P., Guenet, B., Helfenstein, J., Huang, Y., Lauerwald, R., Maignan,
976 F., Naipal, V., Wang, Y., Yang, H., and Zhang, H.: Global evaluation of the nutrient-enabled version of
977 the land surface model ORCHIDEE-CNP v1.2 (r5986), Geosci. Model Dev., 14, 1987–2010,
978 https://doi.org/10.5194/gmd-14-1987-2021, 2021.

979 Tebaldi, C. and Knutti, R.: The use of the multi-model ensemble in probabilistic climate projections,
980 Philos. Trans. R. Soc. Math. Phys. Eng. Sci., 365, 2053–2075, 2007.

981 Terrer, C., Prentice, I., Jackson, R., Keenan, T., Kaiser, C., Vicca, S., Fisher, J., Reich, P., Stocker, B.,
982 Hungate, B., Penuelos, J., McCallum, I., Soudzilovskala, N., Cernusak, L., Talhelm, A., Van, S. K., Piao,
983 S., Newton, P., Hovenden, M., Blumenthal, D., Liu, Y., Muller, C., Winter, K., Field, C., Viechtbauer,
984 W., Van, L. C., Hoosbeek, M., Watanabe, M., Koike, T., Leshyk, V., Polley, W., and Franklin, O.:
985 Nitrogen and phosphorus constrain the CO_2 fertilization of global plant biomass, Nat. Clim. Change, 9,
986 684–689, https://doi.org/10.1038/s41558-019-0545-2, 2019.

987 Thomas, R. Q., Brookshire, E. N. J., and Gerber, S.: Nitrogen limitation on land: How can it occur in
988 Earth system models?, Glob. Change Biol., 21, 1777–1793, https://doi.org/10.1111/gcb.12813, 2015.

989 Tian, H., Chen, G., Lu, C., Xu, X., Hayes, D. J., Ren, W., Pan, S., Huntzinger, D. N., and Wofsy, S. C.:
990 North American terrestrial CO_2 uptake largely offset by CH_4 and N_2O emissions: toward a full accounting
991 of the greenhouse gas budget, Clim. Change, 129, 413–426, https://doi.org/10.1007/s10584-014-1072-9,
992 2015.

993 Tian, H., Yang, J., Lu, C., Xu, R., Canadell, J. G., Jackson, R., Arneth, A., Chang, J., Chen, G., Ciais, P.,
994 Gerber, S., Ito, A., Huang, Y., Joos, F., Lienert, S., Messina, P., Olin, S., Pan, S., Peng, C., Saikawa, E.,
995 Thompson, R. L., Vuichard, N., Winiwarter, W., Zaehle, S., Zhang, B., Zhang, K., and Zhu, Q.: The
996 Global N_2O Model Intercomparison Project (NMIP), Bull. Am. Meteorol. Soc., 99, 1231–1251,
997 https://doi.org/10.1175/BAMS-D-17-0212.1, 2018.

998   Tian, H., Xu, R., Canadell, J. G., Thompson, R. L., Winiwarter, W., Suntharalingam, P., Davidson, E. A.,
999   Ciais, P., Jackson, R. B., Janssens-Maenhout, G., Prather, M. J., Regnier, P., Pan, N., Pan, S., Peters, G.
1000 P., Shi, H., Tubiello, F. N., Zaehle, S., Zhou, F., Arneth, A., Battaglia, G., Berthet, S., Bopp, L.,
1001 Bouwman, A. F., Buitenhuis, E. T., Chang, J., Chipperfield, M. P., Dangal, S. R. S., Dlugokencky, E.,
1002 Elkins, J. W., Eyre, B. D., Fu, B., Hall, B., Ito, A., Joos, F., Krummel, P. B., Landolfi, A., Laruelle, G. G.,
1003 Lauerwald, R., Li, W., Lienert, S., Maavara, T., MacLeod, M., Millet, D. B., Olin, S., Patra, P. K., Prinn,
1004 R. G., Raymond, P. A., Ruiz, D. J., Werf, G. R. van der, Vuichard, N., Wang, J., Weiss, R. F., Wells, K.
1005 C., Wilson, C., Yang, J., and Yao, Y.: A comprehensive quantification of global nitrous oxide sources and
1006 sinks, Nature, 586, 248–256, https://doi.org/10.1038/s41586-020-2780-0, 2020.

1007 Tian, H., Bian, Z., Shi, H., Qin, X., Pan, N., Lu, C., Pan, S., Tubiello, F. N., Chang, J., Conchedda, G.,
1008 Liu, J., Mueller, N., Nishina, K., Xu, R., Yang, J., You, L., and Zhang, B.: History of anthropogenic
1009 Nitrogen inputs (HaNi) to the terrestrial biosphere: a 5 arcmin resolution annual dataset from 1860 to
1010 2019, Earth Syst. Sci. Data, 14, 4551–4568, https://doi.org/10.5194/essd-14-4551-2022, 2022.

1011 Todd-Brown, K. E. O., Randerson, J. T., Post, W. M., Hoffman, F. M., Tarnocai, C., Schuur, E. A. G.,
1012 and Allison, S. D.: Causes of variation in soil carbon simulations from CMIP5 Earth system models and

1013 comparison with observations, Biogeosciences, 10, 1717–1736, https://doi.org/10.5194/bg-10-1717-2013,
1014 2013.

1015 Townsend, P. A., Serbin, S. P., Kruger, E. L., and Gamon, J. A.: Disentangling the contribution of
1016 biological and physical properties of leaves and canopies in imaging spectroscopy data, Proc. Natl. Acad.
1017 Sci., 110, E1074–E1074, https://doi.org/10.1073/pnas.1300952110, 2013.

1018 U.S. Department of Agriculture: World Agricultural Production, U.S. Department of Agriculture, 2022.

1019 Verger, A., Baret, F., and Weiss, M.: Near Real-Time Vegetation Monitoring at Global Scale, IEEE J.
1020 Sel. Top. Appl. Earth Obs. Remote Sens., 7, 3473–3481, https://doi.org/10.1109/JSTARS.2014.2328632,
1021 2014.

1022 Vicca, S., Stocker, B. D., Reed, S., Wieder, W. R., Bahn, M., Fay, P. A., Janssens, I. A., Lambers, H.,
1023 Peñuelas, J., Piao, S., Rebel, K. T., Sardans, J., Sigurdsson, B. D., Sundert, K. V., Wang, Y. P., Zaehle,
1024 S., and Ciais, P.: Using research networks to create the comprehensive datasets needed to assess nutrient
1025 availability as a key determinant of terrestrial carbon cycling, Environ. Res. Lett., 13, 125006,
1026 https://doi.org/10.1088/1748-9326/aaeae7, 2018.

1027 Vitousek, P. M., Menge, D. N., Reed, S. C., and Cleveland, C. C.: Biological nitrogen fixation: rates,
1028 patterns and ecological controls in terrestrial ecosystems, Philos. Trans. R. Soc. B Biol. Sci., 368,
1029 20130119, https://doi.org/10.1098/rstb.2013.0119, 2013.

1030 Vuichard, N., Messina, P., Luyssaert, S., Guenet, B., Zaehle, S., Ghattas, J., Bastrikov, V., and Peylin, P.:
1031 Accounting for carbon and nitrogen interactions in the global terrestrial ecosystem model ORCHIDEE
1032 (trunk version, rev 4999): multi-scale evaluation of gross primary production, Geosci Model Dev, 12,
1033 4751–4779, https://doi.org/10.5194/gmd-12-4751-2019, 2019.

1034 Walker, A. P., Beckerman, A. P., Gu, L., Kattge, J., Cernusak, L. A., Domingues, T. F., Scales, J. C.,
1035 Wohlfahrt, G., Wullschleger, S. D., and Woodward, F. I.: The relationship of leaf photosynthetic traits -
1036 Vcmax and Jmax - to leaf nitrogen, leaf phosphorus, and specific leaf area: A meta-analysis and modeling
1037 study, Ecol. Evol., 4, 3218–3235, https://doi.org/10.1002/ece3.1173, 2014.

1038 Wang, R., Goll, D., Balkanski, Y., Hauglustaine, D., Boucher, O., Ciais, P., Janssens, I., Penuelas, J.,
1039 Guenet, B., Sardans, J., Bopp, L., Vuichard, N., Zhou, F., Li, B., Piao, S., Peng, S., Huang, Y., and Tao,
1040 S.: Global forest carbon uptake due to nitrogen and phosphorus deposition from 1850 to 2100, Glob.
1041 Change Biol., 23, 4854–4872, https://doi.org/10.1111/gcb.13766, 2017.

1042 Wang, S., Zhang, Y., Ju, W., Chen, J. M., Ciais, P., Cescatti, A., Sardans, J., Janssens, I. A., Wu, M.,
1043 Berry, J. A., Campbell, E., ..., and Penuelas, J.: Recent global decline of CO_2 fertilization effects on
1044 vegetation photosynthesis, Science, 370, 1295–1300, https://doi.org/10.1126/science.abg4420, 2020a.

1045 Wang, Y. P., Law, R. M., and Pak, B.: A global model of carbon, nitrogen and phosphorus cycles for the
1046 terrestrial biosphere, Biogeosciences, 7, 2261–2282, https://doi.org/10.5194/bg-7-2261-2010, 2010.

1047 Wang, Z., Tian, H., Yang, J., Shi, H., Pan, S., Yao, Y., Banger, K., and Yang, Q.: Coupling of
1048 Phosphorus Processes With Carbon and Nitrogen Cycles in the Dynamic Land Ecosystem Model: Model
1049 Structure, Parameterization, and Evaluation in Tropical Forests, J. Adv. Model. Earth Syst., 12,
1050 e2020MS002123, https://doi.org/10.1029/2020MS002123, 2020b.

1051   Wieder, W.: Regridded Harmonized World Soil Database v1.2,
1052   https://doi.org/10.3334/ORNLDAAC/1247, 2014.

1053   Wieder, W., Cleveland, C., Lawrence, D., and Bonan, G.: Effects of model structural uncertainty on
1054   carbon cycle projections: Biological nitrogen fixation as a case study, Environ. Res. Lett., 10, 044016,
1055   https://doi.org/10.1088/1748-9326/10/4/044016, 2015a.

1056   Wieder, W., Cleveland, C. C., Smith, W. K., and Todd-Brown, K.: Future productivity and carbon storage
1057   limited by terrestrial nutrient availability, Nat. Geosci., 8, 441–444, https://doi.org/10.1038/ngeo2413,
1058   2015b.

1059   Wieder, W., Lawrence, D. M., Fisher, R. A., Bonan, G. B., Cheng, S. J., Goodale, C. L., Grandy, A. S.,
1060   Koven, C. D., Lombardozzi, D. L., Oleson, K. W., and Thomas, R. Q.: Beyond Static Benchmarking:
1061   Using Experimental Manipulations to Evaluate Land Model Assumptions, Glob. Biogeochem. Cycles, 33,
1062   1289–1309, https://doi.org/10.1029/2018GB006141, 2019.

1063   Wiltshire, A. J., Burke, E. J., Chadburn, S. E., Jones, C. D., Cox, P. M., Davies-Barnard, T.,
1064   Friedlingstein, P., Harper, A. B., Liddicoat, S., Sitch, S., and Zaehle, S.: JULES-CN: a coupled terrestrial
1065   carbon–nitrogen scheme (JULES vn5.1), Geosci Model Dev, 14, 2161–2186,
1066   https://doi.org/10.5194/gmd-14-2161-2021, 2021.

1067   Wright, S. J., Turner, B. L., Yavitt, J. B., Harms, K. E., Kaspari, M., Tanner, E. V. J., Bujan, J., Griffin,
1068   E. A., Mayor, J. R., Pasquini, S. C., Sheldrake, M., and Garcia, M. N.: Plant responses to fertilization
1069   experiments in lowland, species-rich, tropical forests, Ecology, 99, 1129–1138,
1070   https://doi.org/10.1002/ecy.2193, 2018.

1071   Yang, X., Thornton, P. E., Ricciuto, D. M., and Post, W. M.: The role of phosphorus dynamics in tropical
1072   forests - A modeling study using CLM-CNP, Biogeosciences, 11, 1667–1681, https://doi.org/10.5194/bg-
1073   11-1667-2014, 2014.

1074   Zaehle, S. and Dalmonech, D.: Carbon-nitrogen interactions on land at global scales: Current
1075   understanding in modelling climate biosphere feedbacks, Curr. Opin. Environ. Sustain., 3, 311–320,
1076   https://doi.org/10.1016/j.cosust.2011.08.008, 2011.

1077   Zaehle, S. and Friend, A. D.: Carbon and nitrogen cycle dynamics in the O-CN land surface model: 1.
1078   Model description, site-scale evaluation, and sensitivity to parameter estimates, Glob. Biogeochem.
1079   Cycles, 24, https://doi.org/10.1029/2009GB003521, 2010.

1080   Zaehle, S., Medlyn, B. E., Kauwe, M. G. D., Walker, A. P., Dietze, M. C., Hickler, T., Luo, Y., Wang, Y.
1081   P., El-Masri, B., Thornton, P., Jain, A., Wang, S., Warlind, D., Weng, E., Parton, W., Iversen, C. M.,
1082   Gallet-Budynek, A., Mccarthy, H., Finzi, A., Hanson, P. J., Prentice, I. C., Oren, R., and Norby, R. J.:
1083   Evaluation of 11 terrestrial carbon-nitrogen cycle models against observations from two temperate Free-
1084   Air CO2 Enrichment studies, New Phytol., 202, 803–822, https://doi.org/10.1111/nph.12697, 2014.

1085   Zaehle, S., Jones, C. D., Houlton, B., Lamarque, J. F., and Robertson, E.: Nitrogen availability reduces
1086   CMIP5 projections of twenty-first-century land carbon uptake, J. Clim., 28, 2494–2511,
1087   https://doi.org/10.1175/JCLI-D-13-00776.1, 2015.

1088   Zechmeister-Boltenstern, S., Keiblinger, K. M., Mooshammer, M., Peñuelas, J., Richter, A., Sardans, J.,
1089   and Wanek, W.: The application of ecological stoichiometry to plant-microbial-soil organic matter
1090   transformations, Ecol. Monogr., 85, 133–155, https://doi.org/10.1890/14-0777.1, 2015.

1091   Zhang, Y. and Liang, S.: Fusion of Multiple Gridded Biomass Datasets for Generating a Global Forest
1092   Aboveground Biomass Map, Remote Sens., 12, 2559, https://doi.org/10.3390/rs12162559, 2020.

1093   Zhang, Y., Xiao, X., Wu, X., Zhou, S., Zhang, G., Qin, Y., and Dong, J.: A global moderate resolution
1094   dataset of gross primary production of vegetation for 2000-2016, Sci. Data, 4, 1–13,
1095   https://doi.org/10.1038/sdata.2017.165, 2017.

1096   Zheng, M., Zhou, Z., Luo, Y., Zhao, P., and Mo, J.: Global pattern and controls of biological nitrogen
1097   fixation under nutrient enrichment: A meta-analysis, Glob. Change Biol., 25, 3018–3030,
1098   https://doi.org/10.1111/gcb.14705, 2019.

1099   Zheng, M., Zhou, Z., Zhao, P., Luo, Y., Ye, Q., Zhang, K., Song, L., and Mo, J.: Effects of human
1100   disturbance activities and environmental change factors on terrestrial nitrogen fixation, Glob. Change
1101   Biol., 26, 6203–6217, https://doi.org/10.1111/gcb.15328, 2020.

1102